Sustainable Food Technology

ROYAL SOCIETY OF CHEMISTRY

PAPER

View Article Online
View Journal | View Issue

Cite this: *Sustainable Food Technol.*, 2026, 4, 3168

Development of pectin/pullulan-based freshness indicator films incorporated with hibiscus anthocyanin and cassava peel cellulose nanofiber-stabilized Pickering nanoemulsion

Nurin Afzia and Tabli Ghosh *

With evolving market demands, there is a critical need to transcend beyond conventional petroleum-based packaging strategies, as their extensive use has led to serious environment-related issues. In response, a new generation of intelligent packaging systems has been developed to enable continuous monitoring of packaged foods and to provide real-time information on their quality and safety status. Within this context, in the present study, multifunctional freshness indicator films of pectin and pullulan were fabricated, wherein anthocyanin rich hibiscus extract (AHE) and tea tree oil loaded Pickering emulsions (PEs) were intricately incorporated into the biopolymeric pectin/pullulan matrix. Furthermore, the developed films were analyzed for their structural, physicochemical, barrier, optical, color stability, ammonia vapor sensitivity and antioxidant activities. X-ray diffraction of the films showed a wide peak at 21.47° (2θ), suggesting specific structural characteristics. Physicochemical analysis showed an increase in thickness (0.17 ± 0.015–0.49 ± 0.015 mm), followed by decrease in moisture content (22.78 ± 0.42% to 15.40 ± 0.28%) and water absorption (60.71 ± 0.50% to 24.62 ± 0.34%). The pectin/pullulan/PE/AHE film exhibited a tensile strength of 8.43 ± 0.48 MPa and an elongation at break of 69.50 ± 3.14%, along with the highest antioxidant activity (43.52 ± 0.23%). When tested for ammonia vapor sensitivity, the films showed significant color change (ΔE > 53), indicating their potential for real time freshness monitoring quality. Furthermore, the indicator films were also evaluated for the real time freshness of chicken meat. In general, this study provides valuable insights in formulating composite films with anthocyanin and PE, contributing to multifunctional packaging systems with enhanced functionality and greater utility in the food business.

Received 28th October 2025
Accepted 15th February 2026

DOI: 10.1039/d5fb00754b

rsc.li/susfoodtech

Sustainability spotlight

This study represents a sustainable approach for developing multifunctional freshness indicator films using pectin/pullulan biopolymer matrix integrated with anthocyanin-rich hibiscus extract and tea tree oil-loaded Pickering emulsions stabilized by cassava peel-derived cellulose nanofibers. The conversion of cassava peel-based agro-waste into functional materials is aligned with the circular bioeconomy. The developed films exhibited enhanced structural, barrier and antioxidant properties, along with a distinct colorimetric response to ammonia vapor and chicken meat spoilage, enabling real-time freshness monitoring. By combining plant-derived bioactives and Pickering emulsions, the research demonstrates how biopolymer composites can provide both environmental and functional benefits. This innovation not only supports waste utilization and reduces dependence on synthetic packaging but also advances the design of intelligent, biodegradable systems that ensure food quality and safety, contributing to a more sustainable and technologically progressive packaging industry.

Introduction

"Packaging" represents a combination of art, science, and technology, fundamentally designed to uphold the quality, safety, and structural integrity of a product. It constitutes a systematic and strategic approach to prepare commodities for transportation, protection from environmental hazards, distribution, storage, retail presentation, and reduction of financial waste.[1,2] Since the onset of globalization and urbanization, there has been a growing consumer inclination toward food products that meet high safety and quality standards. In recent times, food deterioration has been considered as a serious concern due to its adverse consequences. These consequences range from reduction of nutritional value to the offensive emission of toxic volatiles, which finally lead to significant economic losses. Hence, the economic implications related to food spoilage have now assumed utmost significance in ensuring public health and economic losses.[3] However, in

Department of Food Engineering and Technology, School of Engineering, Tezpur University, Assam, 784028, India. E-mail: tabli@tezu.ernet.in; tablighosh1@gmail.com

previous years, the assessment of food quality has relied on high-cost techniques such as RFID-tags, integrity sensors, time-temperature indicators and other electrochemical sensors, including e-noses, e-tongues, *etc.* Furthermore, these methods are quite complex and not readily available for use by the general public and thus unsuitable for direct incorporation within the packaging system.[4,5] Hence, there is a critical need for simple and affordable approaches applicable from supermarket stores to household settings, enabling direct consumer level quality assessment.[6]

In recent years, the development of intelligent packaging has drawn significant interest as a promising approach for monitoring food freshness.[7] According to a report by the Freedonia group, the market for active and intelligent packaging in the United States was growing rapidly, with the intelligent packaging segment projected to reach approximately $1.5 billion, highlighting its increasing adoption and significance within the packaging industry.[4] Based on this market demand, various studies have explored the use of synthetic pH-sensitive dyes in plastic films to check freshness of perishable foods such as fresh-cut green bell peppers, lean pork, and tilapia.[8–10] While these pH sensitive plastic films are effective, their widespread use has raised significant environmental concerns. This is primarily due to their non-biodegradable nature, which causes environmental accumulations and serious ecological damage.[11] Furthermore, the dyes used for freshness detection could be toxic and contaminate food upon direct contact with it.[12] So, it's important to look into eco-friendly substitutes that lessen the environmental degradation and align with green practices. In this context, natural pigments are considered as an excellent alternative of synthetic dyes as they can give quick and clear visual cues about the freshness of food.[13,14] Notably, many plant extracts, such as curcumin, anthocyanin, tannins, quercetin and carotenoid, can act as natural pigments and replace synthetic dyes such as methyl red and bromocresol.[5,15–17] Among these, anthocyanin, a water-loving phenolic compound, is a good indicator because of its π-conjugated structure, which allows it to absorb visible and ultraviolet light well.[13,15] The hydroxyl and methoxy groups on the aromatic ring of anthocyanin can influence the color modulation through electronic interactions and stabilization of its charged states. As a result, the anthocyanin molecule undergoes structural transitions, shifting from a red flavylium cation to a blue quinoidal base, a colorless carbinol pseudo base, or a yellow chalcone, depending on the surrounding pH conditions.[15]

Among the various anthocyanin sources, hibiscus (*Hibiscus rosa-sinensis*) is recognized as a significant natural source of anthocyanin, which serves as a natural coloring agent in food, cosmetics, pharmaceuticals and dyes. Among the various anthocyanins found in red hibiscus, cyanidin-3-sophoroside is the most prominent pigment.[18] However, the choice of solvent and extraction method for these types of natural pigments has a significant impact for maximizing the yield. In recent years, the use of green solvents has gained significant attention as an eco-friendly substitute for conventional solvents. They offer enhanced efficiency and stability in the extraction of bioactive compounds including anthocyanins.[19] Among the different green solvents, glycerol is one of the green solvents derived from natural sources with great extraction efficiency, biodegradability, and non-toxicity. On the other hand, the ultrasound-assisted extraction (UAE) technique is considered as a promising green extraction technique. This technique has efficient recovery of desired bioactive compounds such as anthocyanin, phenolic acids and flavonoids, by utilizing its unique cavitation mechanism.[20–22] This technique remarkably shortens the extraction time, whereas, at the same time, enhancing both the quality and yield of the resulting extract. Additionally, the process can reduce the dependence on organic solvents, thus lessening the environmental impact of extraction procedures.[21] The optimization of UAE parameters is important to increase the efficiency of extraction while reducing economic and environmental effects. Thus, developing a sustainable and efficient extraction strategy for anthocyanins is very much essential.[20]

Besides, the use of anthocyanin in biopolymer-based films exhibits responsiveness to nitrogenous compounds such as amines and ammonia, owing to nitrogen-induced discoloration.[23,24] Moreover, in order to integrate such sensors within sustainable packaging systems, biopolymeric matrices such as pectin and pullulan are especially suitable. These matrices have remarkable film forming capability, functionality and intrinsic biodegradability. The synergistic use of such biopolymeric systems is of great potential in the creation of high-performance packaging solutions.[25]

Furthermore, incorporation of essential oils has the potential to strengthen the color stability of anthocyanin. This improvement is linked to their rich composition of bioactive compounds, including alcohols, esters and phenols. These compounds not only contribute to color stabilization but also impart notable antioxidant and antimicrobial properties.[26,27] Among various essential oils, tea tree oil (TTO), derived from the leaves of *Melaleuca alternifolia*, exhibits broad-spectrum antioxidant and antibacterial properties, rendering it a potent bioactive agent. Notably, it has significant efficacy against a wide range of microbial pathogens, including *Pseudomonas aeruginosa*, *Escherichia coli*, and various fungal species, making it a valuable bioactive compound for various applications.[28,29] However, the direct use of these free essential oils in composite films tend to reduce the activity resulting from continuous diffusion and loss of volatile materials. Moreover, phase separation and immiscible behavior caused due to essential oil adversely influence the transparency of films.[30,31] Hence, in order to overcome all these difficulties, Pickering emulsions (PEs), which can be stabilized by solid particles, have been used as a viable method for encapsulating essential oils.[32] Unlike conventional emulsions, which often experience instability, PEs offer enhanced structural integrity due to their unique stabilization mechanism. This enhanced stability is intricately linked to the absorption of nanoparticles at the oil–water interface, which effectively forms a protective barrier around the oil droplets, preventing coalescence and Ostwald ripening. Furthermore, the solid particles used for stabilization can be sourced from natural and biodegradable materials, making them a sustainable alternative to synthetic stabilizers.[33] Among these, cellulose nanofibers (CNFs) have been extensively

investigated as eco-friendly solid particles with potential applications as emulsion stabilizers.[34] This is due to their elongated fibrous structure, which forms an interconnected network that enhances the emulsion stability. This network acts as a protective barrier around oil droplets, effectively preventing their coalescence and maintaining the integrity of emulsion stability.[35] As a result, CNFs offer a promising and sustainable solution for stabilizing emulsions in various applications.

This research therefore aims to develop a freshness indicator film by incorporating anthocyanin extracted from *Hibiscus rosa-sinensis* and tea tree oil-loaded PEs into a pullulan/pectin matrix. The physicochemical properties, functional properties, structural properties, antioxidant activity, antimicrobial properties, and pH-stability of the fabricated films were systematically assessed. To establish its practical applicability, the developed film was employed as a freshness indicator for chicken meat, demonstrating its potential for real-time monitoring of food quality.

Materials and methods

Materials

For this study, hibiscus (*Hibiscus rosa-sinensis*) petals were collected from the local area of Tezpur University, Tezpur, Assam, India. Glycerol anhydrous (extrapure AR, 99.5%) was purchased from Sisco Research Laboratories Pvt. Ltd, Maharashtra, India. Furthermore, Loba Chemie Pvt. Ltd, Mumbai, India supplied the ultrapure pectin and Tokyo Chemical Industry Co., Ltd, Tokyo, Japan supplied the pullulan (PO978). Furthermore, for the analytical purpose, potassium chloride and sodium acetate were supplied by Sigma-Aldrich, Tokyo, Japan. Folin–Ciocalteu reagent, gallic acid, and 2,2-diphenyl-1-picrylhydrazyl (DPPH) were provided by Sisco Research Laboratory Pvt. Ltd, Maharashtra, India. Sodium carbonate was received from Avantor Performance Materials India Pvt. Ltd, Mumbai, India. All the chemicals used in the experiments were of analytical grade. However, cut chicken meat was purchased from a local chicken shop near Tezpur University, Tezpur, Assam.

Methods

Ultrasound-assisted extraction of anthocyanin from red hibiscus petals. For the extraction, red hibiscus petals were cleaned with distilled water and then dried at 35 °C for 24 h. Subsequently, the dried petals were ground and sieved to collect the fine powder. Furthermore, the glycerol–water mixture was prepared following the methodology as described by Kowalska *et al.*,[36] with some minor modifications. Specifically, glycerol was taken at varying concentrations and mixed with distilled water. The resulting mixture was stirred at 40 °C for 1 h to disperse glycerol effectively.

A precisely measured 1 wt% hibiscus powder was added into 50 mL of the glycerol–water mixture (S/L ratio 1 : 50). UAE was carried out using an IG-96A ultrasonic cell disruption system (iGene Labserve Pvt. Ltd), operating at a fixed frequency of 21 kHz. Amplitude and sonication time were regulated under pre-established conditions to maximize extraction efficiency. After the extraction step, the resulting mixture was centrifuged at 6000 rpm for 30 min in a high speed centrifuge (Make: Eppendorf, Germany, Model:5430R). The centrifugation process facilitated the separation of solid residues, allowing the collection of the supernatant for further analysis.

Optimization of process parameters for anthocyanin extraction. For the optimization of process parameters for effective extraction of anthocyanin, a Central Composite Rotatable Design (CCRD) was utilized in order to acquire the experimental design with three independent variables *viz.* extraction time (A), amplitude (B), and glycerol concentration (C), with anthocyanin content (X) as the dependent variable. The extraction time was systematically varied between 6 and 15 min, corresponding to coded levels of −1.68 (6 min), −1 (∼8.00 min), 0 (∼11.00 min), +1 (∼13.00 min) and +1.68 (15 min). The ultrasonic amplitude was adjusted within the range of 30% to 70%, representing coded levels of −1.68 (30%), −1 (∼38%), 0 (∼50%), +1 (∼62%) and +1.68 (70%). Similarly, the glycerol concentration was varied between 30 and 80%, with coded levels of −1.68 (30%), −1 (∼40%), 0 (∼55%), +1 (∼70%) and +1.68 (80%). A total of 20 experimental runs were conducted to achieve optimization, as depicted in Table 1. The experimental design was based on the CCRD methodology, which necessitates 2^k factorial points ($k = 3$, $2^k = 2^3 = 8$, core design points) in this study. Additionally, the design included $2k$ axial or star points ($k = 3$, $2k = 2 \times 3 = 6$, outside the core region). Furthermore, six replicate runs at the centre points were included to estimate the pure error. To determine the anthocyanin content at the optimum level, State-Ease 360 @ software was used. Moreover, to fit the experimental data, a second order polynomial equation was used as represented in eqn (1).

$$X = \alpha_0 + \Sigma\alpha_i P_i + \Sigma\alpha_{ii} P_i^2 + \Sigma\alpha_{ij} P_i P_j \quad (1)$$

where α_0 indicates the coefficient constant; α_i, α_{ii} and α_{ij} stand for regression coefficients; P_i and P_j indicate the independent variables; X represents the response or anthocyanin content.

Analysis of variance (ANOVA) was employed to test the factors that significantly influenced the model. Furthermore, the validity and predictive power of the model were assessed based on some diagnostic measures, such as the lack of fit test, coefficient of determination (R^2) and measure of adequacy in precision. A statistically non-significant lack of fit ($p > 0.05$) and an adequacy in precision value greater than a cut-off of 4 suggest the robustness and reliability for prediction.[37] Response surface plots were used to examine the impact of interaction between the process variables on the content of anthocyanin. Furthermore, optimization of the production process was performed through a multi-response desirability function system to identify the optimum conditions.

Analysis of the anthocyanin rich hibiscus extract (AHE)

Total anthocyanin content (TAC). Total anthocyanin content of the red hibiscus extract was determined spectrophotometrically using the pH differential method. This method is intended to measure the structural shift in the anthocyanin chromophore

Table 1 Various experimental conditions and their responses for anthocyanin extraction

Run	*A*: Time (min)	*B*: Amplitude (%)	*C*: Glycerol (%)	*Z*: Anthocyanin content (mg C3G per 100 g)
1	7.82 (∼8.00)	38.11 (∼38.00)	40.13 (∼40.00)	523.62
2	10.50 (∼11.00)	50.00	80.00	450.14
3	10.50 (∼11.00)	70.00	55.00	494.12
4	10.50 (∼11.00)	50.00	55.00	577.62
5	7.82 (∼8.00)	61.89 (∼62.00)	40.13 (∼40.00)	536.32
6	13.18 (∼13.00)	38.11 (∼38.00)	69.87 (∼70.00)	524.43
7	10.50 (∼11.00)	50.00	55.00	576.62
8	15.00	50.00	55.00	637.03
9	13.18 (∼13.00)	38.11 (∼38.00)	40.13 (∼40.00)	697.09
10	10.50 (∼11.00)	50.00	55.00	582.1
11	10.50 (∼11.00)	50.00	30.00	646.18
12	10.50 (∼11.00)	50.00	55.00	592.26
13	10.50 (∼11.00)	50.00	55.00	554.77
14	6.00	50.00	55.00	475.6
15	10.50 (∼11.00)	30.00	55.00	596.33
16	13.18 (∼13.00)	61.89 (∼62.00)	69.89 (∼70.00)	482.1
17	10.50 (∼11.00)	50.00	55.00	550.19
18	13.18 (∼13.00)	61.89 (∼62.00)	40.13 (∼40.00)	633.68
19	7.82 (∼8.00)	38.11 (∼38.00)	69.87 (∼70.00)	480.8
20	7.82 (∼8.00)	61.89 (∼62.00)	69.87 (∼70.00)	417.13

in order to quantify the total monomeric anthocyanin that occurs between pH 1.0 and pH 4.5.[38] Here, two different dilutions of the extracted test samples (1 mL) were prepared using 0.025 M potassium chloride (KCl) and 0.4 M sodium acetate ($CH_3COONa \cdot 3H_2O$) buffer solution. Furthermore, hydrochloric acid (HCl) was used to adjust the buffers to pH 1.0 and pH 4.5, respectively. Finally, the absorbance at 530 and 700 nm was measured using a Carry Series UV-Vis Spectrophotometer (MAKE#AGILENT TECHNOLOGIES, USR; MODEL#CARRY 100), with a blank solution containing glycerol. TAC was expressed in terms of milligram per 100 grams (mg C3G per 100 g) of the dried red hibiscus and was determined using eqn (2) and (3):

$$\mathrm{TAC(mg\ C3G\ per\ L)} = \frac{A \times \mathrm{M.W.} \times \mathrm{DF} \times 1000}{\varepsilon \times L} \quad (2)$$

$$\mathrm{TAC(mg\ C3G\ per\ 100\ g)} = \frac{\mathrm{TAC(mg\ C3G\ per\ L)} \times \mathrm{sample\ volume(mL)}}{\mathrm{sample\ weight(g)} \times 10} \quad (3)$$

where A (absorbance) = $(A_{530} - A_{700})$ pH 1.0 − $(A_{530} - A_{700})$ pH 4.5, M.W. denotes the molecular weight of cyanidin-3-glucoside (449.2 g mol^{-1}); DF corresponds to the dilution factor; ε signifies the molar absorptivity coefficient of cyanidin-3-glucoside (26 900 L cm^{-1} mol^{-1}); and L represents the optical path length of the cuvette in cm.

Total phenolic content (TPC). TPC of the optimized AHE was quantified using the Folin–Ciocalteu (FC) method as described by Rizkiyah *et al.*[39] At first, to dilute the FC reagent, distilled water was used at a dilution ratio of 1 : 10. For the analysis, 0.5 mL of the extracted sample was aliquoted into a test tube and mixed with 1 mL of diluted FC reagent. The solution mixture was subsequently maintained for 10 min prior to the addition of 4 mL of 7.5% (w/v) sodium carbonate. Following this, the solution was kept for a period of 30 min, without being disturbed. Spectrophotometric analysis was then conducted to record the absorbance at 765 nm. TPC was quantified and expressed as milligrams of gallic acid equivalent (GAE) per 100 g of dried red hibiscus (mg GAE per 100 g). To facilitate this quantification, a gallic acid standard curve was established using concentrations ranging from 0.01 mg mL^{-1} to 0.1 mg mL^{-1}.

Total flavonoid content (TFC). The TFC was quantified spectrophotometrically and expressed as milligrams of quercetin equivalent (mg QE) per 100 g of the sample, utilizing the technique employed by Anis and Ahmed[40] with slight modifications. For the analysis, an equal volume (200 μL each) of distilled water and 5% (m/v) sodium nitrite solution was mixed with 500 μL of hibiscus extract. The mixture was subsequently treated with 300 μL of 10% (m/v) aluminium chloride after incubating in the dark for 5 min. Following this, 1000 μL (1 mL) of 1 M sodium hydroxide and 1000 μL (1 mL) of distilled water were successively added to the mixture for achieving uniformity. After a total reaction time of 15 min, the absorbance was taken at 510 nm using a Carry Series UV-Vis Spectrophotometer (MAKE#AGILENT TECHNOLOGIES, USR; MODEL#CARRY 100). A solvent consisting of a glycerol–water mixture was used as the blank.

DPPH radical scavenging activity

The free radical scavenging activity of the optimized AHE was assessed using the 2,2-diphenyl-1-picrylhydrazyl (DPPH) radical scavenging method as outlined by Kaur and Qadri.[41] Following the method, DPPH solution (0.1 mM) was prepared freshly in methanol in a controlled dark environment. For the assay, 0.1 mL of the extract was mixed with 3.9 mL of DPPH solution and the mixture was again kept in the dark for 30 min. The absorbance was recorded spectrophotometrically at 517 nm, against a glycerol–water mixture as the blank. The scavenging

activity was expressed in terms of % inhibition and was calculated using eqn (4)

$$\text{DPPH radical scavenging activity } (\%) = \frac{A_{\text{blank}-} A_{\text{sample}}}{A_{\text{blank}}} \times 100 \quad (4)$$

where A_{blank} is the absorbance of the blank; A_{sample} is the absorbance of the sample.

UV-vis spectroscopic analysis

UV-vis spectroscopy of the optimized AHE was performed using a Carry Series UV-Vis Spectrophotometer (MAKE#AGILENT TECHNOLOGIES, USR; MODEL#CARRY 100). The absorbance was measured in the range of 200–800 nm and the pH value varies from 2–13 to observe absorption spectra.

Fabrication of CNFs

CNFs were fabricated from cassava peel-based cellulose as mentioned in the study conducted by Afzia, Bora, and Ghosh, (2025).[25] Cellulose was extracted from cassava peel by alkali treatment (4% NaOH, 90 °C, 2 h,400 rpm), followed by bleaching with 4% NaOCl (80 °C, 2 h) and purification using 2% H_2O_2. The obtained cellulose after drying was treated with 50 wt% H_2SO_4 for 2 h. Afterwards, cold water was added to stop the reaction, followed by centrifugation (6000 rpm, 20 min, 27 °C), homogenization (10 000 rpm, 10 min), sonication and dialysis. Finally, freeze drying (−50 °C, 24 h) was performed to obtain the CNFs.

Formulation of the tea tree oil-based PE

In this study, the PE was formulated by mixing tea tree oil with a CNF suspension at a predetermined ratio of 1 : 9. Prior to the emulsification process, CNFs were dispersed in distilled water and ultrasonicated for 5 min at 50% amplitude to prepare a stable CNF suspension. Here, the concentration of CNFs was adjusted to 1 wt%, 3 wt%, 5 wt%, 10 wt%, and 15 wt%. Following this, tea tree oil was incorporated dropwise into the aqueous phase and subjected to high-shear homogenization for 5 min at 10 000 rpm. Furthermore, to remove the air bubbles trapped within the PE, the final suspension was again ultrasonicated for 5 min, followed by homogenization for 1 min to achieve a uniform emulsion structure.

Type of the formulated PE

The type of the Pickering emulsion was assessed through the drop test method as described by Yue *et al.*[42] For the analysis, 1 mL aliquot of the emulsion was introduced into 10 mL of distilled water. Afterwards, the dispersion behaviour of the emulsion droplets was observed. Uniform dispersion of emulsion droplets within the aqueous medium signified an oil-in-water (O/W) emulsion, while a water-in-oil (W/O) emulsion remained localized at the interface without any significant dispersion in the aqueous medium.

Optical microscopic analysis

Optical analysis of the formulated PE was observed using a Trinocular microscope (Make: KARL ZEISS, GERMANY; MODEL: AXIOSTAR) attached with a digital camera. To capture high resolution images, a single drop of the emulsion was placed on a microscope slide and evenly spread using another slide. The optical analysis of the emulsion droplet was observed at a magnification of 10×.

Particle size analysis

The particle size analysis of the developed PE was measured through dynamic laser scattering using a Zetasizer Pro (Malvern Panalytical, United Kingdom). Initially, a small droplet of PE was diluted with distilled water at a dilution ratio of 0.2 : 20 (μL mL^{-1}), followed by ultrasonication for 5 min. Particle size measurement was conducted at a scattering angle of 172.9°, within a measurement range of 0.3 nm −10 μm.

Storage stability

To evaluate the storage stability, the creaming index (CI) of the PE was determined by measuring the ratio of the serum layer height (H_s) to the total height of the PE (H_t) as shown in eqn (5).[42]

$$\text{CI}(\%) = \frac{H_s}{H_t} \times 100\% \quad (5)$$

Development of freshness indicator films

The development of the freshness indicator film was accomplished through the solution casting method with some minor modifications.[30] Initially, 2 wt% of pullulan solution was formulated by subjecting it to continuous stirring on a Stuart hotplate stirrer (UC152D) for 30 min, maintaining a controlled temperature of 30 °C. Subsequently, the temperature was increased to 60 °C prior to the addition of pectin into the solution. Then, the PE of tea tree oil (5% v/v of the solution) and AHE (10 wt%), which was already extracted using glycerol, were added into the pullulan/pectin matrix and stirred at 60 °C for another 30 min. The resulting film-forming solution was subsequently subjected to homogenization at 10 000 rpm for 5 min. Thereafter, the homogenized mixture was cast into a Petri dish (90 × 15 mm) and dried at 40 °C to develop the freshness indicator film. Once dried, the film was gently removed and stored in a desiccator for conditioning prior to subsequent characterization and analysis. A pullulan/pectin (PP) control film without the AHE and PE was prepared. In addition, various other film formulations were developed, including a pullulan/pectin composite with the Pickering emulsion (PP_PE) and pullulan/pectin along with AHE (PP_AHE) for comparative analysis. All the films were prepared according to the previously described procedure. The formulation and corresponding codes for each film sample was mentioned below in Table 2.

Table 2 Compositions for the developed pullulan/pectin-based films

Sl no.	Pullulan (wt%)	Pectin (wt%)	PE (5% v/v)	AHE (10 wt%)	Nomenclature
1	2	2	No	No	PP
2	2	2	Yes	No	PP_PE
3	2	2	No	Yes	PP_AHE
4	2	2	Yes	Yes	PP_PE_AHE

Characterization of the developed films

X-ray diffraction (XRD). The crystal structure of the synthesized PP, PP_PE, PP_AHE and PP_PE_AHE films were studied using X-ray diffraction (XRD) analysis. Characterization was conducted using D8 FOCUS and MINIFLEX X-ray diffractometer models to measure the diffraction patterns of the materials. Measurements of diffraction were carried out in the angular range of 5° to 80° (2θ) with a step size of 0.5°. For processing and analyzing the diffraction data obtained, advanced software programs such as XRD COMMANDER 2, DIFFRACEVA, and Rigaku software were employed. The analytical methods offered extensive information about the crystalline features of the CNF-based nanocomposite films.

Fourier transform infrared spectroscopy (FTIR). The infrared spectra of the synthesized PP, PP_PE, PP_AHE and PP_PE_AHE films were measured using a SPECTRUM100 and FORNTIER IR spectrophotometer over a spectral range of 400–4000 cm^{-1} with a scanning speed of 8 scans per second to establish the structural and compositional features of the films.

Thickness. A digital vernier caliper (ABS Digimatic Caliper, Mitutoyo, Japan; measuring range: 0–100 mm) was used to measure the film thickness, and the results were expressed as mean ± standard deviation to increase measurement precision.

Color and transparency. The color attributes (L^*, a^*, b^*) and the total color difference (ΔE) of the developed films were analyzed using a Hunter color Lab (Ultra-Scan VIS, Hunter Lab, USA), as described by Afzia, Bora, and Ghosh, 2025.[25] The ΔE values were measured by considering the PP film as the reference standard and calculated using eqn (6). Furthermore, the optical transparency of the films was evaluated using a UV-vis spectrophotometer (MAKE#AGILENT TECHNOLOGIES, USR; MODEL#CARRY 100), operating across a spectral range of 200 to 800 nm. For the analysis, film samples were precisely cut into standardized dimensions of 10 mm × 40 mm to ensure uniformity across all the measurements.

$$\Delta E = \sqrt{(\Delta L^*)^2 + (\Delta a^*)^2 + (\Delta b^*)^2} \quad (6)$$

Mechanical properties

The tensile strength, elongation at break, and Young's modulus of the developed films were evaluated using a texture analyser (TA-HD Plus Serial no. # 5187; Stable Micro System, UK) equipped with a 5 kg load cell.[25] Prior to analysis, the films were precisely cut into strips measuring 10 mm × 40 mm to ensure uniformity in testing. Mechanical testing was conducted under specified conditions, including a pre-test speed of 5 mm s^{-1}, a test speed of 0.5 mm s^{-1}, a post assessment velocity of 5 mm s^{-1}, 15 mm of displacement and a 5 g of trigger force. Each experimental group underwent five repetitions to enhance the reliability and reproducibility of the measured parameters.

Moisture content (MC)

To determine the MC of the developed PP, PP_PE, PP_AHE and PP_PE_AHE films, film samples were precisely cut into dimensions of 0.04 × 0.04 m^2. These samples were subsequently subjected to a controlled drying process in a hot air oven (Model: IG 95HAO, IGENELABSERVE) maintained at 105 °C for a continuous period of 24 h to ensure complete moisture removal. The moisture content was quantified using the equation described by Afzia, Bora, and Ghosh, 2025.[25]

Water vapor transmission rate (WVTR)

In compliance with ASTM standard E398-03, WVTR was assessed using the cup method.[43] In this process, the cups filled with anhydrous calcium chloride (0% RH) were enclosed with the developed films. However, thickness of the films and surface area of the cups were carefully measured prior to the analysis. Furthermore, the sealed permeation cells, containing the films, were subsequently placed inside a desiccator maintained at 75% relative humidity (RH) using saturated sodium chloride solution. The whole setup was remained undisturbed for 24 h at 23 °C. Following the test period, the WVTR value was calculated by recording the weight change of the permeation cell relative to the surface area and time, and expressed in terms of percentage.[25]

Antioxidant activity

The antioxidant activity of the developed PP, PP_PE, PP_AHE and PP_PE_AHE films was assessed using the 2,2-diphenyl-1-picrylhydrazyl (DPPH) radical scavenging method as outlined by Zhao *et al.*,[44] with minor modifications. As per the specified procedure, 0.1 g of the prepared film was introduced into 10 mL of distilled water and subjected to continuous magnetic stirring to facilitate extraction. Furthermore, DPPH solution (0.06 mol m^{-3}) was prepared freshly in ethanol in a controlled dark environment. For the assay, 2 mL aliquot of the film extract was mixed with 2 mL of DPPH solution and the resulting mixture was incubated in the dark for 30 min. The absorbance was measured spectrophotometrically at 517 nm against a blank of ethanol. The antioxidant activity was expressed in terms of % DPPH free radical scavenging activity and was calculated using eqn (7).

$$\text{Free radical scavenging activity}(\%) = \left(1 - \frac{A_{\text{sample}} - A_{\text{blank}}}{A_{\text{sample}}}\right) \times 100 \quad (7)$$

where A_{blank} is the absorbance of the control; A_{sample} is the absorbance of the sample.

Ammonia vapor sensitivity test or color response to ammonia

The colorimetric response of the developed films to volatile ammonia (NH_3) was assessed based on the method described

by[45] Mohseni *et al.*, with minor modifications. Film samples were cut into 0.02 m × 0.03 m pieces and positioned 0.02 m above the 0.008 mol L^{-1} ammonia solution at room temperature (25 ± 2 °C) for 20 min. Afterwards, the total ΔE value was calculated using the standard eqn (6) to quantify the extent of colorimetric change.

pH stability of indicator films

The pH sensitivity of the developed films was investigated by monitoring the color changes over a 5 days storage period. For the test, the films were immersed into the buffer solutions whose pH values varied from pH 2 to 12 according to the procedure provided by Qin *et al.*[46] The ΔE generated in the films was determined quantitatively using a Hunter color Lab (UltraScan VIS, Hunter Lab, USA).

Storage study on chicken meat

The developed colorimetric films (PP_AHE and PP_PE_AHE) were cut into 0.02 m × 0.02 m pieces and adhered to the inner surface of a transparent plastic container. After that, freshly obtained chicken meat samples were subjected to boiling for 1 min to reduce the initial surface microbial load. The samples were then aseptically placed inside the containers, which were then stored under refrigerated condition at 4 °C for a period of 10 days. To evaluate the storage assessment, chicken meat pieces were analyzed on the basis of weight loss, pH change, color properties and microbial analysis. Apart from this, the progression of color change in the embedded indicator films were monitored at predetermined intervals (0, 2, 4, 6, and 10 days) throughout the storage period. Weight loss of the chicken meat samples was quantified over 2, 4, 6, and 10 days. For pH assessment, chicken meat was homogenized for 10 s, followed by centrifugation, and the resulting supernatant was subjected to pH analysis using a digital pH meter (model: HANNA). Colorimetric evaluation of both the chicken meat and indicator films was performed using a HunterLab UltraScan VIS spectrophotometer (HunterLab, USA), capturing key parameters indicative of quality and spoilage. Further, total plate count was quantified based on the pour plate method, capturing key parameters indicative of quality and spoilage.

Statistical analysis

The data set was subjected to statistical analysis utilizing IBM SPSS Statistics software (version 20), employing one-way analysis of variance (ANOVA). Subsequent post hoc evaluations were performed using Duncan's multiple range test to ascertain statistically significant differences at $p < 0.05$.

Results and discussion

Optimization of process parameters for anthocyanin extraction

Model fitting. Table 3 illustrates the experimental response values corresponding to different combinations of input variables. Based on the data, second order polynomial equations were developed and respective regression coefficients for the coded variables were estimated. The significance of the process parameters influencing anthocyanin content was evaluated through the ANOVA table, as summarized in Table 3. Furthermore, statistical validation of the developed model was assessed through R^2 value, lack of fit and adequacy precision. A combination of non-significant lack of fit and adequate precision greater than 4 suggests the effectiveness of the model in making accurate predictions. The data presented in Table 3 illustrate that, with respect to anthocyanin content, the overall model exhibited statistical significance at $p < 0.05$. The primary factors *A*, *B*, and *C* along with the interactive factor *AC* and quadratic terms B^2 and C^2 also exhibited significant *p*-values, thereby confirming their substantial influence on the response variables. Furthermore, the model revealed a non-significant lack of fit, as indicated by a *p*-value of 0.3276 ($p > 0.05$) for anthocyanin content. This implies that, the model has accurately captured the experimental data without much deviation from the observed responses. Also, the R^2 obtained from the model developed was 0.9659, implying that nearly 96.59% of the total variability in the observed response data can be explained by the suggested predictive model. This high R^2 value implied a very good correlation between the experimental process variables and the responses measured.

Table 3 ANOVA table for the statistical evaluation of experimental responses for anthocyanin content based on the fitted model

Source	Sum of square	*F* value	*p*-value
Model	95 846.34	31.49	< 0.0001
A-time	31 101.05	91.97	< 0.0001
B-amplitude	7957.36	23.53	0.0007
C-glycerol	48 754.82	0.0001	< 0.0001
AB	374.42	1.11	0.3175
AC	3288.20	9.72	0.0109
BC	381.57	1.13	0.3131
A^2	964.85	2.85	0.1221
B^2	2043.81	6.04	0.0338
C^2	1736.55	5.14	0.0469
Residual	3381.74		
Lack of fit	2041.73	1.52	0.3276
Pure error	1340.00		
Cor total	99 228.07		
R^2	0.9659		
Adequacy in precision	20.24		

The mathematical expression formulated in terms of coded variables is presented as follows:

$$Z = -293.55 + 80.61A + 10.79B + 8.75C - 0.21AB - 0.50AC - 0.03BC - 1.14A^2 - 0.08B^2 - 0.04C^2$$

Effect of interaction of various parameters on anthocyanin content

Response surface plots were utilized to illustrate the influence and interactions of the independent variables—time, amplitude, and glycerol concentration—on the total anthocyanin content. The effects of these parameters on anthocyanin yield

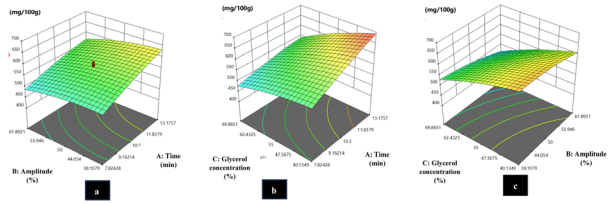

Fig. 1 Effect of the interaction on (a) time and amplitude, (b) time and glycerol concentration, and (c) amplitude and glycerol concentration.

were described using second-order polynomial equations, and the relationships between the variables were represented by 3D response surface graphs (Fig. 1).

Fig. 1(a) illustrates the interactive effects of time (A) and amplitude (B) on the extraction yield of anthocyanin. From the figure, the increase in anthocyanin content has been observed with increase in the ultrasonication time. This phenomenon could be due to the extended interaction between the solvent and solute, thereby increasing the mass transfer efficiency during the UAE process.[47] Conversely, the effect of amplitude demonstrated a more complex behaviour. Anthocyanin content was increased gradually up to an amplitude of ~50%. Under these conditions, the solvent was able to penetrate more deeply and quickly within pores of the cells, due to the acoustic cavitation, which forms bubbles and then collapse in the liquid due to the vibration caused by ultrasound. The collapse of these cavitation bubbles generates intense mechanical forces (called shear stress) that help push the fluid into cells or materials.[48] However, amplitude exceeding this optimal threshold resulted in a decrease in the anthocyanin content. At higher amplitude, the bubbles might collapse more violently, generating higher shear forces, which could degrade the chemical structure of anthocyanin by disrupting its ring structure.[49] Moreover, a simultaneous increase in both the time and amplitude led to a decrease in the anthocyanin content. This might be due to the degradation process linked with the oxidative reaction generated by free radicals during prolonged and intense sonication, ultimately leading to the structural breakdown of anthocyanins.[49]

Fig. 1(b) depicts the graph of the interaction between the ultrasonic time (A) and the glycerol concentration (C) on the level of anthocyanins. From the figure, a significant ($p < 0.05$) increase in anthocyanin content was observed with increasing the ultrasonication time. In contrast, an increase in glycerol concentration, however, caused a slight decrease in anthocyanin content. This was due to an increase in solvent viscosity, which hindered the mass transfer or decreased the diffusion rate, thereby leading to a lower recovery of anthocyanin and other phenolics from the plant matrix.[41] Despite this, the maximum anthocyanin content was found at a glycerol concentration of about 54%, probably due to glycerol's low polarity in reducing the dielectric constant of the solvent system to extract anthocyanin efficiently.[36] Furthermore, a simultaneous increase in glycerol concentration and ultrasonication time caused a gradual decrease in anthocyanin content. This effect was probably due to the higher viscosity of glycerol, which restricts the mass transfer. However, the applied sonication time was maintained within an effective operational range, without any negative effect on anthocyanin stability.

Fig. 1(c) shows the interaction of amplitude (B) and glycerol concentration (C) on anthocyanin content. A progressive increase in amplitude resulted in a relatively stable anthocyanin yield, indicating minimal fluctuation. In contrast, anthocyanin content was found to be reduced with increase in the glycerol concentration. Additionally, the simultaneous increase in both amplitude and glycerol concentration results in a reduction in anthocyanin content. Such reduction could be attributed to the thermal degradation of anthocyanins, possibly caused by increased shear force, which degrades the chemical structure of anthocyanin.[49] At the same time, increased glycerol concentration greatly enhanced the viscosity of the extraction medium, which lowered the solubility of the plant matrix and thus slowed the anthocyanin extraction.[41]

Optimization and validation of process parameters for maximum anthocyanin content

To enhance the anthocyanin yield, the optimization of process variables was conducted using CCRD. This statistical method provided a systematic study and optimized the key process parameters to determine their optimal levels for maximizing the target response.

Among the different combinations produced during the optimization procedure, the sample with the highest desirability score of 1.000 was chosen as the optimal solution. Under the optimized conditions, namely an extraction time of 11.30 (~11.00) min, an ultrasonic amplitude of 41.66 (42.00%) and a glycerol concentration of 54.13 (54.00%), the model predicted an anthocyanin yield of 594.69 mg C3G per 100 g. The results confirmed the accuracy of the model and the efficiency of the optimization parameters in the maximum recovery of anthocyanin. In addition, to verify the reliability and predictive capability of the designed model, validation was carried out by conducting experimental trials using optimal conditions. The experimentally recorded anthocyanin content was observed to be 575.49 ± 1.65 C3G per 100 g. The values were then compared with the respective values predicted by the model. Furthermore, the deviation between the predicted and actual anthocyanin content was determined to be 3.33%. This comparative analysis confirmed the model's effectiveness in accurately estimating the optimal outcomes associated with the three independent variables.

TPC, TFC and DPPH radical scavenging activity of the optimized AHE

TPC, TFC and DPPH scavenging activity associated with the optimized AHE were analysed. Hibiscus extracts using glycerol-water based extraction exhibited a TPC value of 912.87 ± 6.15 mg GAE per 100 g. This result was in close correlation with the findings reported by Wong *et al.* (2010), where *H. rosa-sinensis* was extracted using methanol as solvent and recorded a TPC value of 735 mg GAE per 100 g.[50] Additionally, another study indicated TPC values of 61.45 ± 3.23 mg GAE per 100 g and 59.31 ± 4.31 mg GAE per 100 g when extracted using

methanol and ethanol, respectively.[51] The above results point towards a more efficient extraction process with the glycerol–water system. The higher TPC value obtained through glycerol–water-based extraction was mostly due to the physicochemical properties of glycerol, which enhanced the polarity of solvent, thus improving solubility as well as stability of phenolic compounds. Furthermore, high viscosity and hydrogen bonding of glycerol may also have improved the penetration of the plant matrix, resulting in more efficient mass transfer of bioactive components.[40,52] Additionally, the use of the UAE method further improved the phenolic recovery because of the effect of acoustic cavitation. In this method, the ultrasonic waves propagate within the liquid phase, which leads to the disruption of the cellular matrix, thereby enhancing the penetration of solvent and release of phenolic compounds that are within the cells.[53] The TFC content was found to be 783.37 ± 8.76 mg QE/100 g, reflecting the high content of flavonoid compounds in the glycerol extract. This reflects the efficacy of glycerol as a green solvent for the extraction of polyphenolic compounds, which are renowned for their antioxidant activity. Furthermore, the DPPH radical scavenging activity assesses the capacity of bioactive compounds to neutralize free radicals. The optimized AHE showed a high DPPH scavenging activity value of 87.68 ± 3.21%, indicating the presence of antioxidative phytochemicals in the petals of *Hibiscus rosa-sinensis*. Additionally, this result was in close correlation with the previous findings conducted on *Hibiscus sabdariffa* L. petal extracts[54] and ethanol extracted *Hibiscus rosa-sinensis* L.[55]

UV-vis spectral analysis of optimized AHE

The colour and UV-vis absorption characteristics of AHE across different pH levels (2–13) demonstrate its strong potential as a natural pH indicator, as shown in Fig. 2(a and b).

At extremely acidic pH (pH 2), the extract exhibited a red colour, with a maximum absorption peak at about 517 nm due to the presence of flavylium cations. As the pH increased to 4, the colour of the solution turned orange and the absorption moved to 527 nm. With further increase to near neutral pH (pH 7), the absorption shifted to 581 nm due to the formation of carbinol pseudo-bases and quinonoidal forms through hydration and deprotonation processes. At pH 10, the extract exhibited a khaki color with a peak near 593 nm, although a decline in absorbance intensity was observed. Under strongly alkaline conditions (pH 13), no distinct peak was detected in the visible region, indicating the breakdown of the anthocyanin chromophore and a loss of conjugation, likely due to the formation of chalcone structures. These pH-responsive spectral and colourimetric variations are consistent with the behaviour previously reported in anthocyanin-rich extracts from different varieties of roselle.[56,57]

Type of PEs

The emulsion droplets exhibited uniform and spontaneous dispersion in distilled water, as demonstrated by the drop test. This behaviour confirmed the formation of an oil-in-water (O/W) emulsion. The observed miscibility within the aqueous phase indicates the thermodynamic favourability and stability of the emulsion system, implying that the oil phase was successfully encapsulated within the continuous aqueous phase.

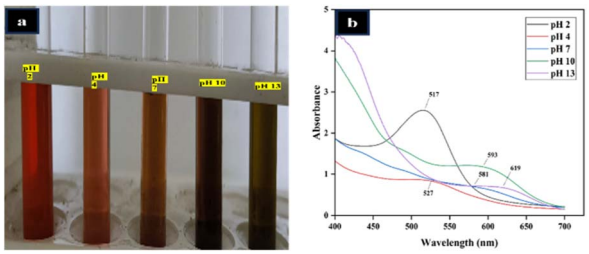

Fig. 2 (a) Effect of pH on the color of anthocyanin-rich hibiscus extract and (b) absorption spectral profiles under varying pH conditions.

Effect of CNF concentrations on PE droplet morphology using optical microscopy and particle size analysis

The microscopic view of the formulated PE is illustrated in Fig. 3(A), which predominantly exhibits well-defined, spherical oil droplets across most of the emulsion variants. A noticeable increase in the overall emulsion volume was observed with the increased concentration of CNFs. This was due to the greater interfacial coverage offered by the CNFs, which enhanced the emulsion stability and reduced the coalescence of droplets. The droplet aggregation was mostly caused by weak intermolecular forces, including van der Waals interactions and hydrophobic attraction between CNF particles, which were responsible for emulsion destabilization. Interestingly, the CNFs in this context appear to function mainly as anti-coalescence agents instead of flocculation inhibitors. Their stabilizing functionality lies in the prevention of droplet merging, although not necessarily preventing droplet proximity or clustering. However, with increasing CNF concentrations, a morphological transformation was observed, wherein small interconnected emulsion droplets aggregated into a more complex network-like structure. This fibrillar matrix, formed by the entanglement of nanofibers at higher loadings, imparted enhanced mechanical rigidity and interfacial integrity, thereby contributing long-term emulsion stability. Among the various formulations, the emulsion stabilized with 15 wt% CNF demonstrated superior colloidal properties, characterized by the smallest average droplet diameter, monodispersity, and the absence of phase separation. This formulation also exhibited a highly uniform and optically homogeneous appearance, as evidenced in Fig. 3A.

Fig. 3B represents the particle size of PEs stabilized with 10 wt% and 15 wt% CNF. The PE containing 10 wt% CNF exhibited the average particle size of 225.7 nm, whereas the PE with 15 wt% CNF displayed an almost similar average particle size of 226.4 nm, which confirmed the formation of nanosized PEs. According to Rigano and Lionetti, 2016, particle sizes between 30 and 1000 nm are indicative of excellent emulsion stability.[58] Since the particle size of the developed PEs also falls

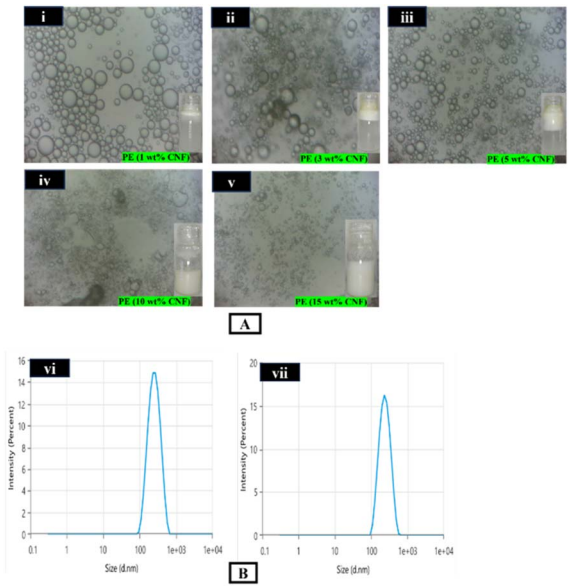

Fig. 3 (A) Effect of CNF concentrations on PE droplet morphology representing PE (1 wt% CNF) (i), PE (3 wt% CNF) (ii), PE (5 wt% CNF) (iii), PE (10 wt% CNF) (iv) and PE (15 wt% CNF) (v). (B) Particle size distribution of PEs prepared with 10 wt% CNF (vi) and 15 wt% CNF (vii).

within this range, they can also be considered as highly stable. Furthermore, the measured particle sizes can also be correlated with the optical appearance of the PEs (Fig. 3(A)), supporting the consistency of the findings.

Evaluation of stabilization behaviour of PEs

To observe the stabilization behaviour of PEs formulated with varying concentrations of CNFs, the CI of all samples was monitored over a 20-day storage period, as summarized in Table 4. A higher CI value is indicative of lower physical stability, whereas a lower CI suggests enhanced resistance to destabilization phenomena such as coalescence, sedimentation, and creaming.

At day 0, the CI values for PE samples containing 1, 3, 5, 10 and 15 wt% CNF were recorded as 59.55 ± 0.05%, 40.00 ± 0.07%, 11.17 ± 0.03%, 0%, and 0%, respectively. These findings demonstrate that increasing the CNF concentration significantly reduced the initial CI, indicating improved emulsion stability. The reduction in CI with increasing CNF concentration was attributed to the ability of CNFs to alter the emulsion phase behaviour by inhibiting droplet aggregation during static storage, thus exerting a synergistic stabilizing effect.[59] Throughout the 20-day storage period, a gradual increase in CI was observed for the lower CNF concentration samples (1, 3 and 5 wt%), suggesting ongoing phase separation and reduced stability over time. In contrast, samples containing 10 wt% and 15 wt% CNF maintained a consistent CI, highlighting their superior long-term stability. These results suggest that CNFs play an important role in both the formation and stabilization of PEs due to their high aspect ratio. However, this was achieved not only through their preferential adsorption at the oil–water interface but also due to their ability to form an interconnected three-dimensional network within the continuous phase, thereby effectively inhibiting the droplet coalescence and creaming.[60]

Visual observations, as shown in Fig. 4, further validate the quantitative data. Emulsions with lower CNF content exhibited the formation of a clear aqueous layer due to creaming, whereas those with higher CNF concentrations showed minimal phase separation. Importantly, the increased CNF content did not lead to undesirable outcomes such as phase separation or precipitation, underscoring the efficacy of CNFs as clean-label, biocompatible stabilizers. These observations are consistent with previous findings by Han *et al.* (2022), who reported a similar stabilization pattern in olive oil-based PEs stabilized with both CNFs and CNCs. Collectively, this study demonstrates that incorporating an optimal CNF concentration is a feasible and effective strategy for enhancing the physical stability of PEs.[59]

Analysis of the developed films

The visual appearance of the developed films is represented in Fig. 5(A), providing a clear representation of their surface features and overall appearance.

FTIR and XRD analysis of the developed films

The FTIR spectra of the pectin/pullulan based films are illustrated in Fig. 5(B-a). In the case of the pure PP and PP_PE films, the broad absorption peak within the range of 3640–3100 cm^{-1} corresponds to the O–H stretching vibrations of hydroxyl groups in the pectin polymer chain. This peak was in close correlation with the peak observed by Priyadarshi *et al.* in 2021.[61] However for the PP_AHE film, the peak became wider due to the incorporation of AHE. This forms new hydrogen bonding with the pectin and pullulan biopolymer matrix.[30] The absorption band observed at 2109 cm^{-1} did not correspond to any characteristic

Table 4 Creaming index of Pickering emulsions stabilized at different CNF concentrations[a]

Sl no.	CNF concentration wt%	CI (%) day 0	CI (%) day 2	CI (%) day 20
1	1	59.55 ± 0.05^{a}	64.44 ± 0.01^{a}	73.33 ± 0.48^{a}
2	3	40.00 ± 0.07^{b}	55.55 ± 0.005^{b}	66.66 ± 0.25^{b}
3	5	11.17 ± 0.03^{c}	24.66 ± 0.03^{c}	44.44 ± 0.21^{c}
4	10	0.00	0.00	0.00
5	15	0.00	0.00	0.00

[a] Note: data are expressed as mean ± SD ($n = 3$), with different superscript letters indicating significant differences ($p < 0.05$).

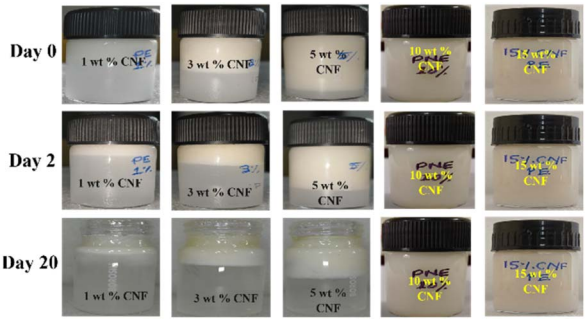

Fig. 4 Visual appearance of CNF-stabilized PEs over storage time.

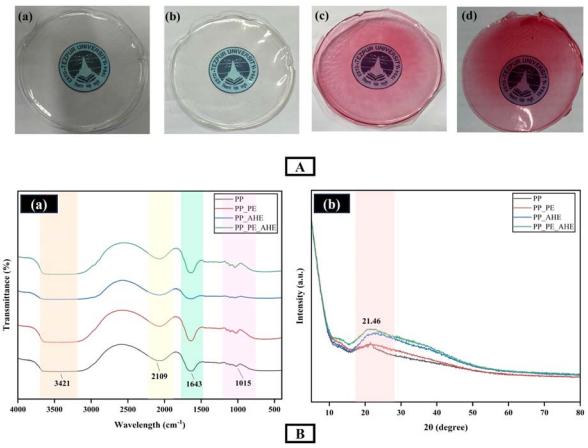

Fig. 5 (A): Visual appearance of the developed (a) PP, (b) PP_PE, (c) PP_AHE (d) PP_PE_AHE films; and (B) FTIR (a) and XRD (b) analysis of the developed films.

functional groups of pectin, pullulan, or anthocyanin compounds. This was likely attributed to an instrumental artifact or noise rather than a chemically meaningful vibration. On the other hand, the strong peak at 1643 cm^{-1} was attributed to the C=O stretching bands corresponding to carboxylic and ester functionalities, characteristic of the asymmetric stretching of carboxylate anions. This validates the occurrence of glucuronic and galacturonic acid residues, which are structural elements of the pectin backbone.[62] This peak also points to probable intermolecular interactions with phenolic compounds in the hibiscus extract.[63] The absorption band at 1015 cm^{-1} was also typical for C–O–C stretching vibrations, commonly originating from glycosidic linkages in polysaccharides. This particular peak aligns with the structural composition of both pullulan and pectin, in accordance with their ether-linked sugar units.[61] However, XRD pattern analysis has not only provided crucial information about the interactions of PP composite films with the PE and AHE but also provided the microstructural order within them, as depicted in Fig. 5(B-b). All types of films exhibited a broad diffraction peak, which was located at approximately 21.46° (2θ), illustrating their nature as mainly amorphous with some crystalline features. The neat PP film exhibited the lowest peak intensity, reflecting a more disordered molecular structure. Furthermore, it has been observed that the AHE incorporation into the PP film increased the amorphous peak compared to the control XRD pattern, implying more amorphous nature due to the presence of anthocyanins. This was likely due to the interference of the native PP interactions, ascribed to hydrogen bonding of anthocyanins with the biopolymer chains.[64] On the other hand, inclusion of the PE and AHE into the matrix resulted in a progressive increase in peak intensity, and the PP_PE_AHE film sample comparatively showed maximum reinforcement. This finding indicates a synergistic interaction allowing partial alignment of the polymer chains or structural reorganization, induced by hydrogen bonding or improved phase compatibility between the biopolymer matrix and added components.[65] Interestingly, no new peak has been observed upon incorporation of the PE and AHE into the films. However, this result corresponds well with the previous study by Shen *et al.*, 2021 on clove essential oil-based PEs and anthocyanin-loaded biocomposites.[65]

Physicochemical, barrier, mechanical and optical properties of the developed films

Thickness. Thickness is considered as one of the key parameters, as it has a significant impact on the properties of the film.[66] Table 5 represents the thickness of the developed PP, PP_PE, PP_AHE and PP_ PE_AHE films, which varied from 0.17 ± 0.015 mm to 0.49 ± 0.015 mm. An increase in film thickness was observed with the incorporation of PE and AHE, which might be due to the well dispersion of the additives in the free space of the PP matrix. Moreover, the presence of functional groups in AHE (*e.g.*, hydroxyl and carbonyl group), in conjugation with the amphiphilic nature of PE and plasticizing nature of glycerol, could form strong intermolecular interactions, which further influenced the film thickness.[57] However, in some

Table 5 Analysis of physicochemical and barrier performance of the developed films[a]

Films	Thickness (mm)	Moisture content (MC) (%)	WVTR ($\times 10^{-3}$ g per m^2 per day)	WA (%)	OA (%)
PP (control)	0.17 ± 0.015^{a}	22.78 ± 0.42^{a}	2.39 ± 0.16^{c}	60.71 ± 0.50^{a}	3.65 ± 0.03^{a}
PP_PE	0.21 ± 0.010^{a}	20.55 ± 0.37^{b}	2.24 ± 0.12^{c}	55.28 ± 0.88^{b}	1.39 ± 0.01^{b}
PP_AHE	0.37 ± 0.010^{b}	16.03 ± 0.50^{c}	4.0 ± 0.10^{a}	30.87 ± 0.56^{c}	0.25 ± 0.01^{c}
PP_ PE_AHE	0.49 ± 0.015^{c}	15.40 ± 0.28^{d}	3.61 ± 0.06^{b}	24.62 ± 0.34^{d}	0.03 ± 0.005^{d}

[a] Note: data are expressed as mean ± SD ($n = 3$), with different superscript letters indicating significant differences ($p < 0.05$).

cases, a high content of anthocyanin could interfere with the orderly arrangement of the polymer chains and disrupt the inner structure of the film matrix, resulting in a subsequent increase in film thickness. Additionally, anthocyanin could also increase the viscosity of the film forming solution, which results in a thicker layer and increased the thickness of the film. In addition to these compositional considerations, the source of anthocyanins, the physicochemical behaviour of the biopolymer utilized, and post-processing storage conditions, specifically relative humidity and light exposure, all have an impact on the thickness of anthocyanin-rich films.[66]

MC, WVTR and WA capacity play a crucial role in evaluating the physical integrity of a film, as all these parameters are directly related to the film's hydrophilicity, barrier performance and overall stability under humid conditions. As evident from Table 5, the incorporation of the PE into the PP film matrix reduced the MC, WVTR and WA of the films as compared to the control PP film. Specifically, MC decreased from 22.78 ± 0.42% in the control PP film to 20.55 ± 0.37% in PP_PE; similarly, WA dropped from 60.71 ± 0.50% to 55.28 ± 0.88%, and WVTR reduced slightly from (2.39 ± 0.16) × 10^{-3} to (2.24 ± 0.12) × 10^{-3} g per m^2 per day. This observed decline could be due to the hydrophobic nature of the tea tree oil and the reinforcing effect of CNFs, which synergistically contribute to the formation of a densely packed and rigid network within the biopolymer matrix. The combined effect of these components likely impedes the diffusion and penetration of water molecules by minimizing the free volume and enhancing the tortuosity of the diffusion path, thereby improving the film's overall water resistance and barrier performance.

Upon incorporation of AHE, a further decrease in MC and WA was observed, with MC reaching 16.03 ± 0.50% and WA decreasing significantly to 30.87 ± 0.56%. This might be ascribed to the presence of abundant hydroxy groups in the anthocyanin molecules, which facilitate extensive intermolecular hydrogen bonding with the hydrophilic domains of the polysaccharide matrix. Additionally, electrostatic interactions between the charged moieties of anthocyanin and the oppositely charged regions of the biopolymeric network further contribute to this behaviour.[66,67] Similar findings have been reported using various anthocyanin-rich sources, including black plum peel,[68] purple corn,[46] and *Lycium ruthenicum* Murr.[69]

Interestingly, while the addition of AHE improved water resistance in terms of MC and WA, a slight increase in WVTR was recorded, ranging from (2.39 ± 0.16) × 10^{-3} g per m^2 per day in the control to (4.00 ± 0.10) × 10^{-3} g per m^2 per day in the PP_AHE film. Although anthocyanins are often reported to reduce WVTR by forming tight molecular interactions that limit water vapor diffusion.[67,70] This anomalous increase may be explained by microstructural imperfections such as pores, cracks, or discontinuities introduced during film casting. These morphological defects can facilitate water vapor transmission, thereby diminishing the barrier properties. Additionally, factors such as the inherent structural complexity of the polysaccharide substrate, the degree of plasticizer–matrix crosslinking, and dispersion of anthocyanins and emulsion droplets play a critical role in determining final WVTR values.[67] In the composite film (PP_PE_AHE), MC and WA were further reduced to 15.40 ± 0.28% and 24.62 ± 0.34%, respectively, confirming the synergistic effect of both PE and AHE in enhancing water resistance. Nonetheless, the WVTR remained moderately high at (3.61 ± 0.06) × 10^{-3} g per m^2 per day, which may again be linked to structural heterogeneity and phase separation within the film matrix.

As shown in Table 5, it was observed that the addition of the PE and AHE reduced the films' ability to absorb oil. Notably, the control film formulated with the PP film exhibited the highest oil absorption. However, with the addition of the PE, the oil absorption value was reduced to 1.39 ± 0.01%, which was further decreased to 0.25 ± 0.01% with the incorporation of AHE. Interestingly, the synergistic integration of both the PE and AHE yielded the most effective barrier, with an oil absorption value minimized to 0.03 ± 0.005%. This substantial decrease could be attributed to the hydrophobic nature of the tea tree oil and the presence of CNFs, which collectively contribute to a dense and less porous film structure that limits oil permeation.

Mechanical behaviour of the developed films

The mechanical properties of films intended for food applications were primarily evaluated through some key parameters such as tensile strength (TS), elongation at break (EAB), and young's modulus (YM). TS reflects the material's ability to resist deformation under stress, while EAB and YM represent the flexibility and stiffness of a film, respectively. Here, the control film (PP) exhibited a tensile strength of 9.79 ± 0.50 MPa, an EAB of 65.80 ± 2.1% and a YM of 14.02 ± 0.59 MPa, as presented in Table 6. Incorporation of the PE significantly enhanced the TS and YM to 11.54 ± 0.45 MPa and 23.42 ± 0.50 MPa, respectively, while EAB was reduced to 49.27 ± 1.8%. This could be due to the rigid and dense network of CNFs, which forms strong intermolecular hydrogen bonding with the hydroxy group of the PP matrix. In contrast to that, films reinforced with AHE (PP_AHE) showed a substantial increase in EAB (74.40 ± 1.9%), but a remarkable decrease in TS (4.48 ± 0.41 MPa) and YM (8.06 ± 0.29 MPa), suggesting enhanced flexibility but reduced structural integrity. The increased flexibility was likely attributed to the presence of phenolic compounds within the AHE, which might act as natural plasticizers and thereby facilitating greater EAB.[57] Furthermore, the combined reinforcement (PP_PE_AHE) resulted in a balanced mechanical profile, with a TS of 8.43 ± 0.48 MPa, an EAB of 69.50 ± 3.14% and a YM of 19.86 ± 0.59 MPa, indicating a synergistic interaction between the PE and AHE that improved the elasticity and stiffness while maintaining moderate tensile strength.

Color properties and transparency of films

The visual appearance of packaging films, particularly their color, plays a critical role in impacting the acceptability of products by consumers, as it not only reflects the aesthetic quality of the film but also signals the detection of freshness and safety of the packaged food. Notably, in anthocyanin rich films, the resulting coloration is highly dependent on the

Table 6 Mechanical behaviour of the developed films[a]

Films	Tensile strength (MPa)	Elongation at break (%)	Young's modulus (MPa)
PP (control)	9.79 ± 0.50^{b}	65.80 ± 2.1^{b}	14.02 ± 0.59^{c}
PP_PE	11.54 ± 0.45^{a}	49.27 ± 1.8^{c}	23.42 ± 0.50^{a}
PP_AHE	4.48 ± 0.41^{d}	74.40 ± 1.9^{a}	8.06 ± 0.29^{d}
PP_PE_AHE	8.43 ± 0.48^{b}	69.50 ± 3.14^{c}	19.86 ± 0.59^{b}

[a] Note: data are expressed as mean ± SD ($n = 3$), with different superscript letters indicating significant differences ($p < 0.05$).

botanical sources of the anthocyanins, giving their diverse molecular structures and pigment profiles. Concurrently, the ability of such films to act as effective barriers against UV-visible light is of importance, as exposure to these wavelengths can accelerate oxidative degradation and compromise the physicochemical stability of food products.[66] Table 7 represents the colorimetric parameters (L^*, a^*, and b^*), total ΔE, and transmittance at 280 nm (T_{280}) and 660 nm (T_{660}), of the developed PP, PP_PE, PP_AHE and PP_ PE_AHE films. The control PP film exhibited the highest lightness (87.55 ± 0.10), minimal redness (0.04 ± 0.005) and a moderate yellowness value (4.57 ± 0.02), with ΔE set as the reference line, reflecting a transparent and colorless appearance. Incorporation of the PE to the film marginally increased the L^* (87.89 ± 0.22) and b^* (5.30 ± 0.02), while maintaining a low a^* value, resulting in a negligible ΔE (0.80 ± 0.02) and suggesting a minimal visual deviation from the control. In contrast, films containing AHE (PP_AHE and PP_ PE_AHE) demonstrated a drastic decline in lightness ($L^* \sim 29$), a significant increase in redness ($a^* > 6.0$) and a shift towards the greenish blue spectrum ($b^* < 0$), with ΔE values exceeding 58, indicative of a pronounced color change likely due to the pigments of AHE.[46]

Furthermore, the UV transmittance at 280 nm was sharply declined in AHE containing films ($14.17 \pm 1.01\%$ for PP_AHE and $15.87 \pm 0.39\%$ for PP_PE_AHE), compared to the control ($75.4 \pm 0.35\%$), suggesting the enhanced UV-blocking capabilities. This might be due to the presence of multiple aromatic rings in the anthocyanin structure, which possess a conjugated π-electron system.[46]

Comparable trends have been consistently reported in the literature, wherein the incorporation of anthocyanin-rich extracts enhanced the UV-visible light barrier properties of the biopolymer-based films. Notably, anthocyanin-rich extracts, such as those obtained from purple corn,[46] black plum extract[68] and *Lycium ruthenicum* Murr,[69] have also been reported to exhibit significant UV-blocking properties. Furthermore, a slight decrease in the visible transmittance at 660 nm was also observed with the incorporation of AHE, from $91.8 \pm 0.81\%$ in the control to $82.73 \pm 1.03\%$ in PP_PE_AHE, indicating potential applications in light-sensitive food packaging.

Antioxidant activity of the developed films

The antioxidant activity of the developed PP, PP_PE, PP_AHE and PP_ PE_AHE films was quantitatively assessed using DPPH radical scavenging assay. Among the formulations, the PP_PE film exhibited a moderate increase in DPPH scavenging activity of $24.26 \pm 0.33\%$ as compared to the control PP film ($20.51 \pm 0.34\%$). This enhancement was due to the presence of key antioxidant terpenes in tea tree oil, including terpinene-4-ol, α-terpinene, α-terpinolene, and γ-terpinene.[71] Furthermore, a pronounced enhancement in DPPH radical scavenging activity was observed upon the incorporation of AHE in the PP film matrix, which was substantially enhanced to $40.64 \pm 0.32\%$. This pronounced improvement in antioxidant activity may be attributed to the presence of a diverse range of phytochemicals, including flavonoids such as quercetin, kaempferol, and myricetin;[72] anthocyanins such as cyanidin-3-glucoside and delphinidin derivatives;[73] as well as phenolic acids including chlorogenic acid, gallic acid, caffeic acid, and protocatechuic.[74] Notably, the PP_PE_AHE film exhibited the optimum radical scavenging activity at $43.52 \pm 0.23\%$, underscoring a synergistic interaction between the bioactive constituents of both the PE and AHE, thereby imparting superior antioxidative functionality to the film matrix.

Colorimetric response of indicator films to volatile NH_3

Table 8 represents the colorimetric parameters (L^*, a^*, and b^*) and total ΔE of different film formulations exposed to ammonia vapor, aiming to assess their potential for intelligent packaging applications through visual color change. Among the four film types tested, only the PP_AHE and PP_PE_AHE formulations showed a distinct color difference when exposed to ammonia

Table 7 Colorimetric and transparency attributes of the developed films[a]

Films	L^*	a^*	b^*	ΔE	T_{280} (%)	T_{660} (%)
PP (control)	87.55 ± 0.10^{a}	0.04 ± 0.005^{b}	4.57 ± 0.02^{c}	0	75.4 ± 0.35^{a}	91.8 ± 0.81^{a}
PP_PE	87.89 ± 0.22^{a}	0.06 ± 0.01^{b}	5.30 ± 0.02^{a}	0.80 ± 0.02^{b}	71.51 ± 0.26^{b}	90.76 ± 0.31^{a}
PP_AHE	29.24 ± 0.41^{b}	6.01 ± 0.38^{a}	-0.26 ± 0.06^{d}	58.82 ± 0.23^{b}	14.17 ± 1.01^{d}	87.70 ± 1.27^{b}
PP_ PE_AHE	28.99 ± 0.68^{b}	6.71 ± 0.11^{a}	-0.21 ± 0.05^{b}	59.14 ± 0.32^{b}	15.87 ± 0.39^{c}	82.73 ± 1.03^{c}

[a] Note: data are expressed as mean ± SD ($n = 3$), with different superscript letters indicating significant differences ($p < 0.05$).

Table 8 Colorimetric response of films to ammonia vapor[a]

Films	L^*	a^*	b^*	ΔE
PP	87.55 ± 0.35^{a}	0.06 ± 0.005^{b}	4.57 ± 0.02^{c}	0.00
PP_PE	87.89 ± 0.29^{b}	0.05 ± 0.04^{b}	5.30 ± 0.02^{a}	0.81 ± 0.01^{c}
PP_AHE	29.08 ± 0.39^{c}	0.99 ± 0.74^{a}	1.92 ± 0.06^{d}	58.49 ± 0.07^{a}
PP_ PE_AHE	33.78 ± 0.33^{b}	0.59 ± 0.54^{a}	4.83 ± 0.05^{b}	53.79 ± 0.24^{b}

[a] Note: data are expressed as mean ± SD ($n = 3$).

vapor. Consequently, these two films were further analyzed for their ΔE values to assess their sensitivity towards volatile alkaline compounds. A higher ΔE value signifies higher response to ammonia vapor. In this study, PP showed no perceptible color change ($\Delta E = 0.00$), whereas the PP_PE film exhibited a minimal color difference of 0.81 ± 0.01. Remarkably, the PP_AHE and PP_PE_AHE films showed drastic color shifts ($\Delta E = 58.49 \pm 0.07$ and 53.79 ± 0.24, respectively), confirming their robust sensitivity to ammonia vapor.

This pronounced ΔE values were attributed to the physicochemical alterations occurring within the indicator film matrix upon exposure to ammonia vapor. When ammonia molecules interact with the water molecules, they undergo hydrolysis and generate hydroxide ions, subsequently increasing the pH value of the surrounding film matrix. This shift towards alkaline conditions caused structural rearrangements in anthocyanin molecules and thereby altering their absorption characteristics in the UV-visible region and resulting in distinct colorimetric changes. Since volatile basic compounds are commonly emitted during the microbial spoilage of proteinaceous food products, these anthocyanin-functionalized films hold considerable promise as real time spoilage indicators for developing next generation intelligent packaging systems.[75]

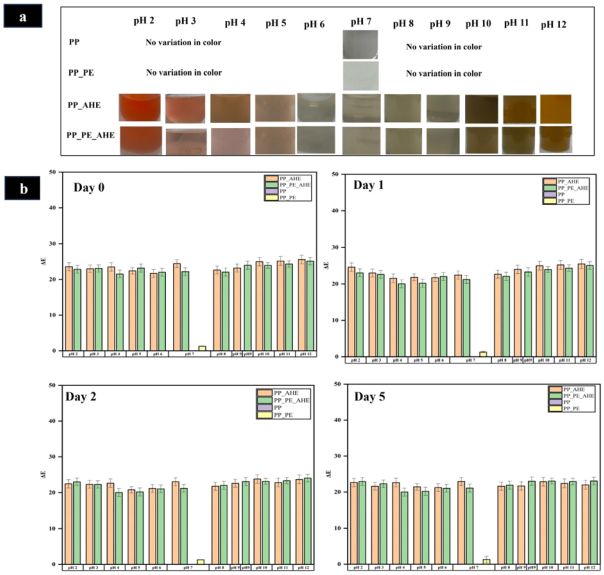

Fig. 6 (a) pH-responsive color transitions and (b) color difference of anthocyanin-based indicator films (pH 2–12).

Color stability of indicator films at different pH

Color stability is a critical parameter for the functional performance of pH-responsive indicator films, particularly for applications in real-time freshness monitoring. In this study, the color stability of the developed anthocyanin-based films (PP_AHE and PP_PE_AHE) was assessed through both visual inspection and instrumental colorimetric analysis (ΔE values) over a 5-day storage period.

As depicted in Fig. 6(a), the films displayed progressive chromatic shifts across the pH spectrum (2–12) on day 0, transitioning from red under acidic conditions to greenish-yellow in alkaline environments, while exhibiting minimal perceptible change at neutral pH. This trend was quantitatively supported by the data presented in Fig. 6(b). The anthocyanin-containing films demonstrated significantly elevated ΔE values under extreme pH conditions, in contrast to the PP_PE control film, which remained chromatically inert across all pH levels. Notably, the ΔE values for both PP_AHE and PP_PE_AHE films remained within the range of 20–25 up to day 5, indicating robust color retention and pH responsiveness. This sustained chromatic stability was due to homogeneous embedding of the anthocyanins within the polymeric network, reducing their exposure to outer degradative conditions and mitigate their denaturation. The structural integrity and physicochemical properties of the film network further helped in maintaining an internally stable microenvironment and consequently shielded the anthocyanin against oxidative and environmental stresses.[76]

Application on chicken meat

The fabricated freshness indicator films (PP_AHE and PP_PE_AHE) were utilized to observe the freshness of slightly boiled chicken meat during the storage period. In this regard, the visual appearance of chicken pieces during refrigerated storage is illustrated in Fig. 7.

Weight loss serves as a key indicator of the physicochemical stability and quality of perishable foods during storage. In the current research, chicken meat sample stored using biopolymer-based indicator films—PP_AHE and PP_PE_AHE—exhibited varying weight loss patterns. As indicated in Fig. 8(a), low weight loss (4.38 ± 0.08 to $5.44 \pm 0.09\%$) was recorded on day 2, showing maximum initial moisture protection. But there was a progressive rise of weight loss from day 4 to day 10, in accordance with the expected preservation dynamics. Specifically, by day 10, the weight loss was found to have increased ($\sim 8.5 \pm 0.09\%$ to $\sim 10 \pm 0.24\%$) due to the evaporation of

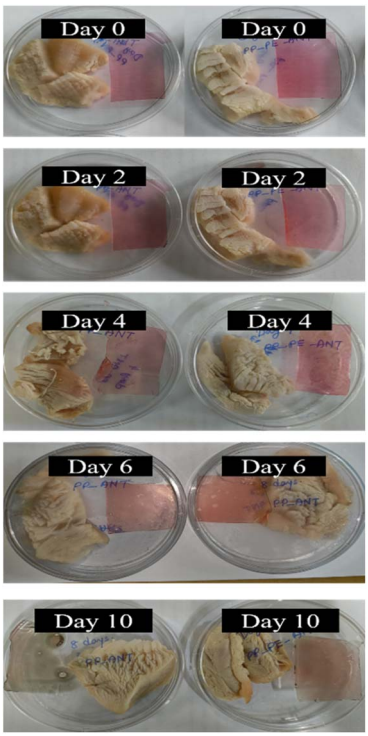

Fig. 7 Visual appearance of the chicken meat over the storage period.

moisture, drip loss associated with protein denaturation and suppressed oxidative lipid decomposition associated with protein.[77] The pH of muscle-based food products, such as chicken meat, serves as a critical biochemical marker during storage, as it directly correlates with microbial spoilage and protein degradation processes. For this study, the initial pH of freshly cooked chicken flesh varied from 5.63 ± 0.02 to 5.67 ± 0.02, indicating a normal postmortem condition. However, as storage progressed, a gradual but consistent rise in pH values was observed, indicating ongoing biochemical and microbial alterations. By day 2, the pH was slightly increased (6.14 ± 0.02 to 6.16 ± 0.03), as a result of microbial growth and enzymatic hydrolysis of proteins, which release basic nitrogen-containing compounds such as ammonia and amines.[78] This increasing trend was persisted up to day 10, as illustrated in Fig. 8(b), reaching a peak range of 6.79 ± 0.06 to 7.05 ± 0.03, reflecting massive protein breakdown and depletion of endogenous glucose, which promoted the formation of volatile basic nitrogen.

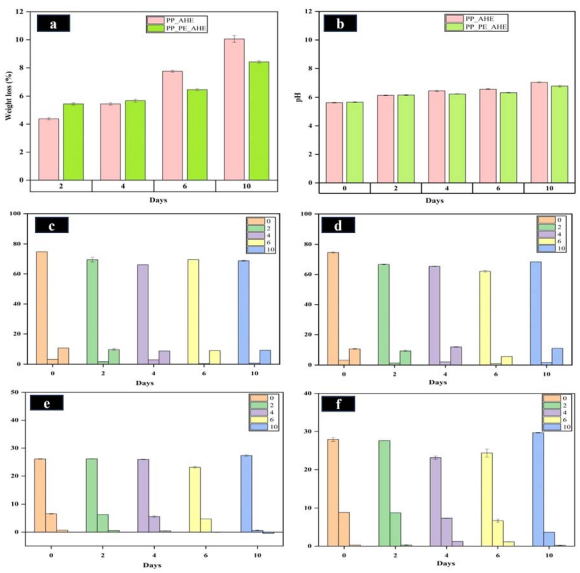

Fig. 8 (a) Weight loss and (b) pH of the chicken meat over the storage period. Color response of chicken meat stored with (c) PP_AHE and (d) PP_PE_AHE-based indicator films and color response of (e) PP_AHE and (f) PP_PE_AHE-based indicator films over the storage time.

Fig. 8(c) and (d) represent the colorimetric parameters (L^*, a^*, and b^*) of chicken meat stored with PP_AHE and PP_PE_AHE-based indicator films, respectively, over 10 days. Initially, both samples showed similar lightness (L^*), redness (a^*), and yellowness (b^*) values. Over time, L^* values generally declined, indicating darkening, with a more pronounced decrease in the PP_PE_AHE group. The a^* values (red-green) dropped significantly, especially in PP_AHE by day 6, suggesting a loss of redness, while PP_PE_AHE showed slightly better color retention. The b^* values (yellow-blue) fluctuated, with PP_PE_AHE peaking on day 4 before a sharp drop by day 6.

However, Fig. 8(e) and (f) show the colorimetric (L^*, a^*, and b^*) changes in PP_AHE and PP_PE_AHE-based indicator films during chicken meat storage over 10 days. Both films exhibited noticeable changes in all three-color parameters, indicating quality deterioration over time. For PP_AHE, L^* remained relatively stable initially but dropped on day 6, then increased on day 10, while a^* and b^* values steadily decreased, even turning negative, indicating loss of redness and a yellow–blue shift. Conversely, the PP_PE_AHE film exhibited a greater decrease in a^* value and an increase in b^* value between day 4 and 6. While an increase in L^* value was observed by day 10, indicating a more distinct color change. These transitions guarantee that both films respond to freshness of meat, with PP_PE_AHE providing more differentiated color variation over time.

Microbial spoilage

Microbial spoilage is a major concern related to chicken meat due to its high perishability under normal as well as refrigerated conditions. In this study, Fig. 9(a and b) represents the changes in total mesophilic and psychrophilic count of the chicken meat throughout the storage period.

On day 0, the mesophilic bacterial count of the chicken meat ranged from 4.09 to 5.04 log 10 (CFU mL^{-1}), while psychrophilic count was in the range of 4.015 to 4.04 log 10 (CFU mL^{-1}). However, a gradual increase in both mesophilic and psychrophilic counts were observed during storage from day 2 to day 10, with the highest count recorded on day 10. By day 10, the mesophilic bacterial count was increased to 9.97–10.47 log 10 (CFU per mL). Similarly, the psychrophilic bacterial count reached 9.27–9.47 log 10 (CFU per mL). Overall, the increase in microbial load correlated well with the visual response of the freshness indicator film, confirming its effectiveness in accurately signalling spoilage of chicken meat during storage.

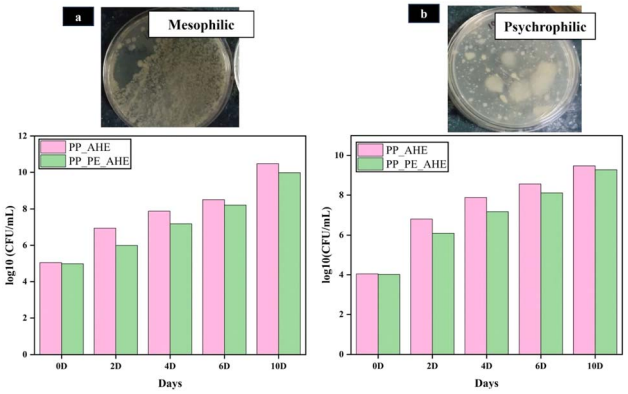

Fig. 9 (a) Mesophilic and (b) psychrophilic bacterial counts of the chicken meat over the storage period with PP_AHE and PP_PE_AHE-based indicator films.

Conclusion

This study highlighted the successful development of a multi-functional freshness indicator film based on a pectin/pullulan biopolymer matrix, anthocyanin-rich hibiscus extract, and tea tree oil-stabilized PE for real-time visual monitoring of chicken meat spoilage. A 15 wt% CNF formulation was discovered to provide the best emulsion system stabilizing performance, with the smallest uniform droplet size distribution. Furthermore, synergistic application of anthocyanins and tea tree oil considerably improved the antioxidant activity of the indicator films due to the intricate phytochemical nature of bioactive compounds. At the same time, incorporation of PE and anthocyanin molecules provided tremendous improvements to the films' barrier properties with implications towards shelf-life enhancement and lesser oxidative degradation of food items. Functionally, the resulting indicator films exhibited a significant and time-dependent colorimetric response in accordance with the consequent deterioration of chicken meat quality. This enables end-users to visually ascertain freshness, onset of decomposition, and stage of spoilage without the need for advanced instrumental analysis. In general, the findings highlighted the importance of a formulation specific strategy that considers the intrinsic properties of the biopolymer matrix and physicochemical interactions of bioactive substances. This approach makes it possible to tailor film performance to suit various applications. Additionally, the integration of advanced characterization techniques and smart material design approaches plays a crucial role in the development of next-generation packaging materials. In summary, the results of this research offer a strong foundation to develop high-performance indicator films, with good potential for both scientific studies and large-scale commercial adoption within the food sector.

Ethical approval

Compliance with ethical approval.

Author contributions

Nurin Afzia: original draft writing, review and editing. Tabli Ghosh: conceptualization, supervision, validation, final review and editing.

Conflicts of interest

The authors declare no conflict of interest.

Data availability

The data can be obtained upon request to the authors.

Acknowledgements

This research was supported by the Start-up Research Grant (SRG) through Science and Engineering Research Board (SERB)-DST, New Delhi, India (SERB File no: SRG/2022/001406).

References

1 F. S. Mohseni-Shahri, F. Moeinpour, S. F. Rafie and N. Abu-Zahra, ZnGlu MOF-enhanced anthocyanin-gelatin films: A novel approach for monitoring chicken meat freshness through experimental and molecular dynamics insights, *Food Chem.*, 2025, **475**, 143380, DOI: 10.1016/j.foodchem.2025.143380.

2 T. Ghosh, K. Mondal and V. Katiyar, Current prospects of bio-based nanostructured materials in food safety and preservation, in *Food Product Optimization for Quality and Safety Control*, Apple Academic Press, 2020, pp. 111–164, DOI: 10.1201/9781003003144-6.

3 W. Chi, L. Cao, G. Sun, F. Meng, C. Zhang, J. Li and L. Wang, Developing a highly pH-sensitive κ-carrageenan-based intelligent film incorporating grape skin powder via a cleaner process, *J. Cleaner Prod.*, 2020, **244**, 118862, DOI: 10.1016/j.jclepro.2019.118862.

4 E. Poyatos-Racionero, J. V. Ros-Lis, J. L. Vivancos and R. Martinez-Manez, Recent advances on intelligent packaging as tools to reduce food waste, *J. Cleaner Prod.*, 2018, **172**, 3398–3409, DOI: 10.1016/j.jclepro.2017.11.075.

5 B. Kuswandi and A. Nurfawaidi, On-package dual sensors label based on pH indicators for real-time monitoring of beef freshness, *Food Control*, 2017, **82**, 91–100, DOI: 10.1016/j.foodcont.2017.06.028.

6 K. B. Biji, C. N. Ravishankar, C. O. Mohan and T. K. Srinivasa Gopal, Smart packaging systems for food applications: a review, *J. Food Sci. Technol.*, 2015, **52**, 6125–6135, DOI: 10.1007/s13197-015-1766-7.

7 F. Moeinpour and F. S. Mohseni-Shahri, Properties of Roselle and alizarin mixed loaded gelatin films as a pH-sensing indicator for shrimp freshness monitoring, *Packag. Technol. Sci.*, 2023, **36**(6), 483–493, DOI: 10.1002/pts.2724.

8 W. Wang, M. Li, H. Li, X. Liu, T. Guo, G. Zhang and Y. Xiong, A renewable intelligent colorimetric indicator based on

polyaniline for detecting freshness of tilapia, *Packag. Technol. Sci.*, 2018, **31**(3), 133–140, DOI: 10.1002/pts.2358.

9 H. Z. Chen, M. Zhang, B. Bhandari and C. H. Yang, Development of a novel colorimetric food package label for monitoring lean pork freshness, *LWT–Food Sci. Technol.*, 2019, **99**, 43–49, DOI: 10.1016/j.lwt.2018.09.048.

10 H. Z. Chen, M. Zhang, B. Bhandari and Z. Guo, Applicability of a colorimetric indicator label for monitoring freshness of fresh-cut green bell pepper, *Postharvest Biol. Technol.*, 2018, **140**, 85–92, DOI: 10.1016/j.postharvbio.2018.02.011.

11 K. L. Law, Plastics in the marine environment, *Annu. Rev. Mar. Sci.*, 2017, **9**(1), 205–229, DOI: 10.1146/annurev-marine-010816-060409.

12 D. Liu, C. Zhang, Y. Pu, S. Chen, L. Liu, Z. Cui and Y. Zhong, Recent advances in pH-responsive freshness indicators using natural food colorants to monitor food freshness, *Foods*, 2022, **11**(13), 1884, DOI: 10.3390/foods11131884.

13 Y. Zhu, X. Gao, X. Gao, Z. Jiang, M. Alhomrani, A. S. Alamri and H. Cui, Development of polysaccharide based intelligent packaging system for visually monitoring of food freshness, *Int. J. Biol. Macromol.*, 2024, **277**, 134588, DOI: 10.1016/j.ijbiomac.2024.134588.

14 Y. Kumar, Y. Bist, D. Thakur, M. Nagar and D. C. Saxena, A review on the role of pH-sensitive natural pigments in biopolymers based intelligent food packaging films, *Int. J. Biol. Macromol.*, 2024, **276**, 133869, DOI: 10.1016/j.ijbiomac.2024.133869.

15 Y. Wang, J. Zhong, D. J. McClements, Z. Zhang, R. Zhang, Z. Jin and L. Chen, Stability enhancement methods for natural pigments in intelligent packaging: a review, *Crit. Rev. Food Sci. Nutr.*, 2024, **65**(29), 6233–6248, DOI: 10.1080/10408398.2024.2437570.

16 T. Ghosh, M. Changmai, and S. Bordoloi, Intelligent packaging—sensors, in *Intelligent Packaging*, Academic Press ,2024, pp. 101–126, DOI: 10.1016/B978-0-443-15388-4.00005-5.

17 K. Lee, S. Baek, D. Kim and J. Seo, A freshness indicator for monitoring chicken-breast spoilage using a Tyvek® sheet and RGB color analysis, *Food Packag. Shelf Life*, 2019, **19**, 40–46, DOI: 10.1016/j.fpsl.2018.11.016.

18 R. Sri Raghavi, M. Visalakshi, S. Karthikeyan, G. Amutha Selvi, S. Thamaraiselvi and K. Gurusamy, Standardisation of anthocyanin extraction techniques from hibiscus (*Hibiscus rosa-sinensis*) petals for biocolour utilisation, *J. Pharm. Innov.*, 2022, **11**(8), 303–309, DOI: 10.22271/tpi.2022.v11.i8d.14647.

19 H. Alasalvar and Z. Yildirim, Ultrasound-assisted extraction of antioxidant phenolic compounds from *Lavandula angustifolia* flowers using natural deep eutectic solvents: An experimental design approach, *Sustainable Chem. Pharm.*, 2021, **22**, 100492, DOI: 10.1016/j.scp.2021.100492.

20 X. Fu, Y. Du, L. Zou, X. Liu, Y. He, Y. Xu, *et al.*, Acidified glycerol as a one-step efficient green extraction and preservation strategy for anthocyanin from blueberry pomace: New insights into extraction and stability protection mechanism with molecular dynamic simulation, *Food Chem.*, 2022, **390**, 133226, DOI: 10.1016/j.foodchem.2022.133226.

21 L. Shen, S. Pang, M. Zhong, Y. Sun, A. Qayum, Y. Liu, *et al.*, A comprehensive review of ultrasonic assisted extraction (UAE) for bioactive components: Principles, advantages, equipment, and combined technologies, *Ultrason. Sonochem.*, 2023, **101**, 106646, DOI: 10.1016/j.ultsonch.2023.106646.

22 R. Martins, A. Barbosa, B. Advinha, H. Sales, R. Pontes and J. Nunes, Green extraction techniques of bioactive compounds: a state-of-the-art review, *Processes*, 2023, **11**(8), 2255, DOI: 10.3390/pr11082255.

23 M. Tavassoli, M. Alizadeh Sani, A. Khezerlou, A. Ehsani, G. Jahed-Khaniki and D. J. McClements, Smart biopolymer-based nanocomposite materials containing pH-sensing colorimetric indicators for food freshness monitoring, *Molecules*, 2022, **27**(10), 3168, DOI: 10.3390/molecules27103168.

24 H. Yousefi, H. Su, S. M. Imani, K. Alkhaldi, C. D. M. Filipe and T. F. Didar, Intelligent food packaging: A review of smart sensing technologies for monitoring food quality, *ACS Sens.*, 2019, **4**(4), 808–821, DOI: 10.1021/acssensors.9b00440.

25 N. Afzia, S. Bora and T. Ghosh, Utilization of cassava-peel based cellulose nanofiber for developing functionalized pectin/pullulan/olive oil nanocomposite film for cling wrapping of chicken meat, *Int. J. Biol. Macromol.*, 2025, **305**, 140879, DOI: 10.1016/j.ijbiomac.2025.140879.

26 A. G. Souza, R. R. Ferreira, L. C. Paula, S. K. Mitra and D. S. Rosa, Starch-based films enriched with nanocellulose-stabilized Pickering emulsions containing different essential oils for possible applications in food packaging, *Food Packag. Shelf Life*, 2021, **27**, 100615, DOI: 10.1016/j.fpsl.2020.100615.

27 M. H. B. Nabi, M. M. Ahmed, M. S. Mia, S. Islam and W. Zzaman, Essential Oils: Advances in Extraction Techniques, Chemical Composition, Bioactivities, and Emerging Applications, *Food Chem. Adv.*, 2025, **8**, 101048, DOI: 10.1016/j.focha.2025.101048.

28 N. Bu, L. Huang, G. Cao, H. Lin, J. Pang, L. Wang and R. Mu, Konjac glucomannan/Pullulan films incorporated with cellulose nanofibrils-stabilized tea tree essential oil Pickering emulsions, *Colloids Surf., A*, 2022, **650**, 129553, DOI: 10.1016/j.colsurfa.2022.129553.

29 T. Jiang, D. Wang, X. Zhang, Q. Yang, Q. Huang, X. Ju and C. Li, Electrospinning of chitosan/polyvinyl alcohol Pickering emulsion with tea tree essential oil loaded for anti-infection wound dressings, *Mater. Chem. Phys.*, 2024, **311**, 128561, DOI: 10.1016/j.matchemphys.2023.128561.

30 H. J. Lim, S. Y. Tang, K. W. Chan, S. Manickam, L. J. Yu and K. W. Tan, A starch/gelatin-based Halochromic film with black currant anthocyanin and Nanocellulose-stabilized cinnamon essential oil Pickering emulsion: Towards real-time Salmon freshness assessment, *Int. J. Biol. Macromol.*, 2024, **274**, 133329, DOI: 10.1016/j.ijbiomac.2024.133329.

31 H. Almasi, S. Azizi and S. Amjadi, Development and characterization of pectin films activated by nanoemulsion

and Pickering emulsion stabilized marjoram (*Origanum majorana* L.) essential oil, *Food Hydrocolloids*, 2020, **99**, 105338, DOI: 10.1016/j.foodhyd.2019.105338.

32 H. Sun, S. Li, S. Chen, C. Wang, D. Liu and X. Li, Antibacterial and antioxidant activities of sodium starch octenylsuccinate-based Pickering emulsion films incorporated with cinnamon essential oil, *Int. J. Biol. Macromol.*, 2020, **159**, 696–703, DOI: 10.1016/j.ijbiomac.2020.05.118.

33 C. Ji and Y. Wang, Nanocellulose-stabilized Pickering emulsions: Fabrication, stabilization, and food applications, *Adv. Colloid Interface Sci.*, 2023, **318**, 102970, DOI: 10.1016/j.cis.2023.102970.

34 A. G. Souza, R. R. Ferreira, L. C. Paula, L. F. Setz and D. S. Rosa, The effect of essential oil chemical structures on Pickering emulsion stabilized with cellulose nanofibrils, *J. Mol. Liq.*, 2020, **320**, 114458, DOI: 10.1016/j.molliq.2020.114458.

35 C. Tang, Y. Chen, J. Luo, M. Y. Low, Z. Shi, J. Tang and K. C. Tam, Pickering emulsions stabilized by hydrophobically modified nanocellulose containing various structural characteristics, *Cellulose*, 2019, **26**, 7753–7767, DOI: 10.1007/s10570-019-02648-x.

36 G. Kowalska, J. Wyrostek, R. Kowalski and U. Pankiewicz, Evaluation of glycerol usage for the extraction of anthocyanins from black chokeberry and elderberry fruits, *J. Appl. Res. Med. Aromat. Plants*, 2021, **22**, 100296, DOI: 10.1016/j.jarmap.2021.100296.

37 N. Afzia, N. Shill, B. J. Kalita and N. Sit, Optimization of conditions for production of pectinase in solid-state fermentation with *Aspergillus flavus* using dried Assam lemon peel powder as substrate, *Meas.: Food*, 2024, **14**, 100166, DOI: 10.1016/j.meafoo.2024.100166.

38 M. R. C. Inácio, K. M. G. de Lima, V. G. Lopes, J. D. C. Pessoa and G. H. de Almeida Teixeira, Total anthocyanin content determination in intact açaí (*Euterpe oleracea* Mart.) and palmitero-juçara (*Euterpe edulis* Mart.) fruit using near infrared spectroscopy (NIR) and multivariate calibration, *Food Chem.*, 2013, **136**(3–4), 1160–1164, DOI: 10.1016/j.foodchem.2012.09.046.

39 D. N. Rizkiyah, N. R. Putra, Z. Idham, M. A. Che Yunus, I. Veza, I. Harny and A. H. Abdul Aziz, Optimization of red pigment anthocyanin recovery from *Hibiscus sabdariffa* by subcritical water extraction, *Processes*, 2022, **10**(12), 2635, DOI: 10.3390/pr10122635.

40 N. Anis and D. Ahmed, Modelling and optimization of polyphenol and antioxidant extraction from *Rumex hastatus* by green glycerol–water solvent according to response surface methodology, *Heliyon*, 2022, **8**(12), e11992, DOI: 10.1016/j.heliyon.2022.e11992.

41 D. Kaur and O. S. Qadri, Green extraction of anthocyanins from *Syzygium cumini* fruit pulp using aqueous glycerol through ultrasound-assisted extraction, *J. Umm Al-Qura Univ. Appl. Sci,.*, 2025, **11**(1), 124–132, DOI: 10.1007/s43994-024-00152-y.

42 M. Yue, M. Huang, Z. Zhu, T. Huang and M. Huang, Effect of ultrasound assisted emulsification in the production of Pickering emulsion formulated with chitosan self-assembled particles: Stability, macro, and micro rheological properties, *LWT–Food Sci. Technol.*, 2022, **154**, 112595, DOI: 10.1016/j.lwt.2021.112595.

43 T. Ghosh and V. Katiyar, Nanochitosan functionalized hydrophobic starch/guar gum biocomposite for edible coating application with improved optical, thermal, mechanical, and surface property, *Int. J. Biol. Macromol.*, 2022, **211**, 116–127, DOI: 10.1016/j.ijbiomac.2022.05.079.

44 R. Zhao, W. Guan, X. Zhou, M. Lao and L. Cai, The physiochemical and preservation properties of anthocyanidin/chitosan nanocomposite-based edible films containing cinnamon-perilla essential oil Pickering nanoemulsions, *LWT–Food Sci. Technol.*, 2022, **153**, 112506, DOI: 10.1016/j.lwt.2021.112506.

45 F. S. Mohseni-Shahri and F. Moeinpour, Development of a pH-sensing indicator for shrimp freshness monitoring: Curcumin and anthocyanin-loaded gelatin films, *Food Sci. Nutr.*, 2023, **11**(7), 3898–3910, DOI: 10.1002/fsn3.3375.

46 Y. Qin, Y. Liu, L. Yuan, H. Yong and J. Liu, Preparation and characterization of antioxidant, antimicrobial and pH-sensitive films based on chitosan, silver nanoparticles and purple corn extract, *Food Hydrocolloids*, 2019, **96**, 102–111, DOI: 10.1016/j.foodhyd.2019.05.017.

47 S. Salacheep, P. Kasemsiri, U. Pongsa, M. Okhawilai, P. Chindaprasirt and S. Hiziroglu, Optimization of ultrasound-assisted extraction of anthocyanins and bioactive compounds from butterfly pea petals using Taguchi method and Grey relational analysis, *J. Food Sci. Technol.*, 2020, **57**, 3720–3730, DOI: 10.1007/s13197-020-04404-7.

48 P. Das, P. K. Nayak and R. Krishnan Kesavan, Ultrasound assisted extraction of food colorants: Principle, mechanism, extraction technique and applications: A review on recent progress, *Food Chem. Adv.*, 2022, **1**, 100144, DOI: 10.1016/j.focha.2022.100144.

49 U. Roobab, A. Abida, G. M. Madni, M. M. A. N. Ranjha, X. A. Zeng, A. M. Khaneghah and R. M. Aadil, An updated overview of ultrasound-based interventions on bioactive compounds and quality of fruit juices, *J. Agric. Food Res.*, 2023, **14**, 100864, DOI: 10.1016/j.jafr.2023.100864.

50 S. K. Wong, Y. Y. Lim and E. W. C. Chan, Evaluation of antioxidant, anti-tyrosinase and antibacterial activities of selected Hibiscus species, *Ethnobot. Leafl.*, 2010, **14**, 781–796.

51 Z. A. Khan, S. A. Naqvi, A. Mukhtar, Z. Hussain, S. A. Shahzad, A. Mansha, *et al.*, Antioxidant and antibacterial activities of *Hibiscus rosa-sinensis* Linn flower extracts, *Pak. J. Pharm. Sci.*, 2014, **27**(3), 469–474.

52 O. Zannou, I. Koca, T. M. Aldawoud and C. M. Galanakis, Recovery and stabilization of anthocyanins and phenolic antioxidants of roselle (*Hibiscus sabdariffa* L.) with hydrophilic deep eutectic solvents, *Molecules*, 2020, **25**(16), 3715, DOI: 10.3390/molecules25163715.

53 N. Medina-Torres, T. Ayora-Talavera, H. Espinosa-Andrews, A. Sánchez-Contreras and N. Pacheco, Ultrasound assisted extraction for the recovery of phenolic compounds from

vegetable sources, *Agronomy*, 2017, **7**(3), 47, DOI: 10.3390/agronomy7030047.

54 A. P. Obouayeba, B. N. Djyh, S. Diabate, A. J. Djaman, J. D. N'guessan, M. Kone and T. H. Kouakou, Phytochemical and antioxidant activity of roselle (*Hibiscus sabdariffa* L.) petal extracts, *Res. J. Pharm., Biol. Chem. Sci.*, 2014, **5**(2), 1453–1465.

55 Y. W. Mak, L. O. Chuah, R. Ahmad and R. Bhat, Antioxidant and antibacterial activities of hibiscus (*Hibiscus rosa-sinensis* L.) and Cassia (*Senna bicapsularis* L.) flower extracts, *J. King Saud Univ. Sci.*, 2013, **25**(4), 275–282, DOI: 10.1016/j.jksus.2012.12.003.

56 T. Senathirajah, S. Rasalingam and S. Ganeshalingam, Extraction of the cyanidin-3-sophoroside from *Hibiscus Rosa-Sinensis*: An efficient natural indicator over a wide range of acid-base titrations, *J. Nat. Prod. Plant Resour.*, 2017, **7**(3), 1–7.

57 J. Zhang, X. Zou, X. Zhai, X. Huang, C. Jiang and M. Holmes, Preparation of an intelligent pH film based on biodegradable polymers and roselle anthocyanins for monitoring pork freshness, *Food Chem.*, 2019, **272**, 306–312, DOI: 10.1016/j.foodchem.2018.08.041.

58 L. Rigano and N. Lionetti, Nanobiomaterials in galenic formulations and cosmetics, in *Nanobiomaterials in Galenic Formulations and Cosmetics*, William Andrew Publishing, 2016, vol. 10, pp. 121–148, DOI: 10.1016/B978-0-323-42868-2.00006-1.

59 Y. Han, R. Chen, Z. Ma, Q. Wang, X. Wang, Y. Li and G. Sun, Stabilization of Pickering emulsions via synergistic interfacial interactions between cellulose nanofibrils and nanocrystals, *Food Chem.*, 2022, **395**, 133603, DOI: 10.1016/j.foodchem.2022.133603.

60 J. Liu, X. Chen and H. Wang, Fabrication of water/oil-resistant paper by nanocellulose stabilized Pickering emulsion and chitosan, *Int. J. Biol. Macromol.*, 2024, **275**, 133609, DOI: 10.1016/j.ijbiomac.2024.133609.

61 R. Priyadarshi, S. M. Kim and J. W. Rhim, Pectin/pullulan blend films for food packaging: Effect of blending ratio, *Food Chem.*, 2021, **347**, 129022, DOI: 10.1016/j.foodchem.2021.129022.

62 E. Santamaría, A. Maestro, S. Chowdhury, S. Vílchez and C. González, Rheological study of pullulan-pectin mixtures to prepare gel beads using the drip method and evaluation as gallic acid release systems, *Food Hydrocolloids*, 2025, **160**, 110747, DOI: 10.1016/j.foodhyd.2024.110747.

63 M. A. Khan, F. Ali, S. Faisal, M. Rizwan, Z. Hussain, N. Zaman, *et al.*, Exploring the therapeutic potential of *Hibiscus rosa sinensis* synthesized cobalt oxide (Co_2O_4-NPs) and magnesium oxide nanoparticles (MgO-NPs), *Saudi J. Biol. Sci.*, 2021, **28**(9), 5157–5167, DOI: 10.1016/j.sjbs.2021.05.035.

64 M. Hasan, A. Utami, C. Siregar, L. Hanum, I. Khaldun and M. Nazar, Thermal, structural and mechanical characterization of bio-nanocomposite films from purple sweet potato starch/chitosan nanoparticles integrated with anthocyanin extract, *Results Eng.*, 2025, **25**, 104448, DOI: 10.1016/j.rineng.2025.104448.

65 Y. Shen, Z. J. Ni, K. Thakur, J. G. Zhang, F. Hu and Z. J. Wei, Preparation and characterization of clove essential oil loaded nanoemulsion and Pickering emulsion activated pullulan-gelatin based edible film, *Int. J. Biol. Macromol.*, 2021, **181**, 528–539, DOI: 10.1016/j.ijbiomac.2021.03.133.

66 H. Yong and J. Liu, Recent advances in the preparation, physical and functional properties, and applications of anthocyanins-based active and intelligent packaging films, *Food Packag. Shelf Life*, 2020, **26**, 100550, DOI: 10.1016/j.fpsl.2020.100550.

67 Y. Li, Z. Hu, R. Huo and Z. Cui, Preparation of an indicator film based on pectin, sodium alginate, and xanthan gum containing blueberry anthocyanin extract and its application in blueberry freshness monitoring, *Heliyon*, 2023, **9**(3), e14421, DOI: 10.1016/j.heliyon.2023.e14421.

68 X. Zhang, Y. Liu, H. Yong, Y. Qin and J. Liu, Development of multifunctional food packaging films based on chitosan, TiO_2 nanoparticles and anthocyanin-rich black plum peel extract, *Food Hydrocolloids*, 2019, **94**, 80–92, DOI: 10.1016/j.foodhyd.2019.03.009.

69 Y. Qin, Y. Liu, H. Yong, J. Liu, X. Zhang and J. Liu, Preparation and characterization of active and intelligent packaging films based on cassava starch and anthocyanins from *Lycium ruthenicum* Murr, *Int. J. Biol. Macromol.*, 2019, **134**, 80–90, DOI: 10.1016/j.ijbiomac.2019.05.029.

70 N. A. Azlim, A. Mohammadi Nafchi, N. Oladzadabbasabadi, F. Ariffin, P. Ghalambor, S. Jafarzadeh and A. A. Al-Hassan, Fabrication and characterization of a pH-sensitive intelligent film incorporating dragon fruit skin extract, *Food Sci. Nutr.*, 2022, **10**(2), 597–608, DOI: 10.1002/fsn3.2680.

71 J. Rudbäck, M. A. Bergström, A. Börje, U. Nilsson and A. T. Karlberg, α-Terpinene, an antioxidant in tea tree oil, autoxidizes rapidly to skin allergens on air exposure, *Chem. Res. Toxicol.*, 2012, **25**(3), 713–721, DOI: 10.1021/tx200486f.

72 A. Purushothaman, P. Meenatchi, S. Saravanan, R. Sundaram and N. Saravanan, Quantification of total phenolic content, HPLC analysis of flavonoids and assessment of antioxidant and anti-haemolytic activities of *Hibiscus rosa-sinensis* L. flowers in vitro, *Int. J. Pharma Res. Health Sci.*, 2016, **4**(5), 1342–1350.

73 G. I. Peredo Pozos, M. A. Ruiz-López, J. F. Zamora Natera, C. Alvarez Moya, L. Barrientos Ramirez, M. Reynoso Silva, *et al.*, Antioxidant capacity and antigenotoxic effect of *Hibiscus sabdariffa* L. extracts obtained with ultrasound-assisted extraction process, *Appl. Sci.*, 2020, **10**(2), 560, DOI: 10.3390/app10020560.

74 J. I. Lyu, J. Ryu, C. H. Jin, D. G. Kim, J. M. Kim, K. S. Seo and S. J. Kwon, Phenolic compounds in extracts of *Hibiscus acetosella* (Cranberry Hibiscus) and their antioxidant and antibacterial properties, *Molecules*, 2020, **25**(18), 4190, DOI: 10.3390/molecules25184190.

75 N. Kanha, R. Jaimun, B. Rattanamato and T. Laokuldilok, Novel indicator film incorporating Dendrobium orchid extract and TiO2 nanoparticles for seafood freshness monitoring, *Future Foods*, 2024, **10**, 100512, DOI: 10.1016/j.fufo.2024.100512.

76 B. Zhu, W. Lu, Y. Qin, G. Cheng, M. Yuan and L. Li, An intelligent pH indicator film based on cassava starch/polyvinyl alcohol incorporating anthocyanin extracts for monitoring pork freshness, *J. Food Process. Preserv.*, 2021, **45**(10), e15822, DOI: 10.1111/jfpp.15822.

77 R. Devi, P. Rasane, S. Kaur and J. Singh, Meat and meat losses: influence on meat quality, *Int. J. Res. Anal. Rev.*, 2019, **6**(1), 762–786.

78 M. Sayadi, A. Mojaddar Langroodi, S. Amiri and M. Radi, Effect of nanocomposite alginate-based film incorporated with cumin essential oil and TiO_2 nanoparticles on chemical, microbial, and sensory properties of fresh meat/beef, *Food Sci. Nutr.*, 2022, **10**(5), 1401–1413, DOI: 10.1002/fsn3.2724.